AMCA COVID Guidance for UNDUCTED Fans – Modeling Ceiling Fans

Prepared for

AMCA INTERNATIONAL
MICHAEL IVANOVICH, SENIOR DIRECTOR

30 West University Drive
Arlington Heights, IL 60004
847 704 6340

Prepared by:

LIANGZHU (LEON) WANG, PHD, PENG
ASSOCIATE PROFESSOR
LEON.WANG@CONCORDIA.CA

SENWEN YANG, PHD CANDIDATE
RUNZHONG (ALVIN) WANG, MASC CANDIDATE
MOHAMMAD MORTEZAZADEH, PHD
JIWEI ZOU, PHD CANDIDATE
CHANG SHU, PHD CANDIDATE

CONCORDIA UNIVERSITY
1455 de Maisonneuve Blvd. W
Montreal, Quebec, Canada H3G 1M8

November 21, 2021

Contents

1. INTRODUCTION

The COVID-19 (SARS-CoV-2) Pandemic has already infected over 202 million people and caused more than 4.2 million deaths worldwide as of August 2021 [1]. The latest research findings show that airborne aerosol transmission contributes to a large portion of the spread of COVID-19 disease, especially in indoor spaces with poor ventilation conditions, large gatherings, and long-duration exposure to high concentration aerosols [2–6]. Several studies show that improving ventilation, wearing a face mask, avoiding overcrowding, and shortening the event time (exposure time) can significantly reduce airborne infection risk in indoor environments [7–9]. Meanwhile, COVID-19 has been showing it can linger longer because of the emerging new variants or possibly become a recurring concern similar to influenza. Therefore, it remains essential to evaluate airborne aerosol transmissions in buildings and suggest mitigation measures for building operations and designs, especially when vaccinations take time and may not provide the expected immunity at the moment. Meanwhile, public health guidelines may relax during the gradual re-opening process.

Ceiling fans are widely used, including smaller diameters ("standard" fans) in residential settings and large diameter ceiling fans (LDCF) in industrial/commercial buildings. Quite a few studies have been undertaken on their airflow and performance characteristics [10–15]. Some studies focused on space ventilation and human thermal comfort, whereas those on airborne pathogen aerosol transmissions in large industrial spaces are limited, especially during the COVID-19 pandemic. Zhu et al. [16] investigated the upper-room ultraviolet germicidal irradiation (UVGI) fixture in a hospital room with a ceiling fan. They found that the UVGI effectively removed the microorganism from the air. One recent study focuses on airborne aerosol transmission in the area under the ceiling fan in a room setup [17]. Meanwhile, ceiling fan-related research was often conducted through experiments of fan types, blade shapes, and rotation speeds. When experimental data are limited, especially during the pandemic, numerical simulations are essential for understanding indoor airborne aerosol/particle transmissions [17–23].

1.1 Objective and challenges

This project supports the effort of "*AMCA* COVID Guidance for Non-Ducted Fans" (hereafter, the Guidance) with the focus on the numerical modeling of ceiling fans. The Guidance responds to the existing and future COVID Guidance from government agencies, customer companies, and health institutions, including the Centers for Disease Control, National Institute for Occupational Health and Safety (NIOSH), American Society of Heating, Refrigerating and Air-Conditioning Engineers (ASHRAE) and Taylor Engineering for Non-Ducted Fans. The Guidance will be externally reviewed by building and health experts to reduce infectious risk, protect members with the early focus on the USA. This report focuses on the numerical simulation studies of airborne particle and aerosol transmission in large warehouses with large diameter ceiling fans.

A few technical challenges have been identified. There are no existing modeling setups and general guidance available for Non-Ducted Fans, such as LDCF, for the airborne transmission risks. Many parameters can be involved, including but not limited to the setups for infector/infected; infector particle release modes, durations, orientations, and the numerical methods to model them; the relative locations of infectors and susceptible, and the fans in space; and the mitigation/abatement strategies for the fan operations. As a result, a parametric study should be conducted, whereas it could be limited by computing costs and resources available. The parametric study also requires justifiable simplifications of the model by steady-state or transient simulations. Finally, it is needed to identify validation cases to support the validity of the numerical simulation setups and

methodologies. The following sections report the simulation methodology, setups, assumptions, validations, and simulation results.

2. METHODS

2.1 Theory - Drift-flux model

When modeling indoor particles, some researchers applied the discrete phase model (DPM), based on the Lagrangian view of fluid to simulate the spreading and deposition of particles [24–26]. However, a DPM simulation is transient, requiring short time steps and substantial computing resources. Based on the Eulerian perspective concept, simulations by tracer species are also an approach for relatively small particles or aerosols [27–30]. Tracer gas is reported as a surrogate of exhaled droplet nuclei to study airborne transmissions in buildings [31], whereas modeling the gravitational and surface depositions has been challenging. Zhu et al. [16] simulated airborne microorganisms as the passive scalar using the Euerlian method in the single-person hospital isolation room with a ceiling fan based on the steady-state airflow field. The simulated space is relatively small (about 42 m^3), and the study did not consider the gravitational and surface depositions of the airborne particles. Another approach to connecting the Lagrangian and Eulerian approach is the "Drift-flux model" [23,32–34], which estimates the depositions with more affordable computing cost than the DPM. Therefore, this research employs the Drift-flux model for the simulations of airborne particle transmissions in large industrial spaces with large diameter ceiling fans.

The governing equation of the particle concentration includes the gravitational settling effect of particles into the convection term in the one-way coupled Drift-flux model. The indoor flow field and temperature fields are solved during the simulation progressed using the standard k−ε model with the standard wall function and the buoyancy effect via the Boussinesq assumption. After the airflow pattern and thermal condition convergence are reached, the particle concentration is solved by Eq. 1 based on the one-way coupled process with the airflow.

$$\frac{\partial(\rho C)}{\partial t} + \nabla \cdot (\rho(\vec{V} + \vec{V}_S)C) = \nabla \cdot (\frac{\mu_{eff}}{\sigma_C}\nabla C) + S_C \quad (1)$$

or

$$\frac{\partial(\rho C)}{\partial t} + \nabla \cdot (\rho(\vec{V} + \vec{V}_S)C) = \nabla \cdot [(D_P + \varepsilon_P)\nabla C] + S_C \quad (2)$$

Where
$\vec{V}_S$ = gravitational settling velocity from the Stokes equation
μ_{eff} = effective viscosity of air, $\mu_{eff} = \mu + \mu_t$
μ = molecular viscosity of air
μ_t = turbulence viscosity, determined from turbulence model
σ_C = Turbulent Schmidt number,$\sigma_C = \frac{\mu_t}{\varepsilon_P}$
D_P = Particle Brownian diffusion coefficient
ε_P= particle turbulent diffusivity

The gravitational settling velocity is determined by

$$|V_S| = C_c\sqrt{\frac{4}{3}\frac{g d_P(\rho_P-\rho)}{C_D\rho}} \quad (3)$$

Where

C_D = drag coefficient; $=\frac{24}{Re}$ for $Re < 1$; $= \frac{24}{Re}(1 + 0.15Re^{\frac{2}{3}})$ for $1 < Re < 1000$

$Re = \frac{\rho_a d_P|V_a-V_P|}{\mu_a}$

ρ_a= air density

d_P = particle diameter

V_P = particle velocity

V_a = air velocity

μ_a=dynamic viscosity of air

The particle deposition mass flux is defined following the modified Fick's law

$$J = v_d C_{cell} = (D_p + \varepsilon_P)\frac{dC}{dy} + iv_s C_{cell} \quad (4)$$

Where *i* is "+" for downward-facing surfaces and "-" for upward-facing surfaces. Numerically, the particle deposition flux for each CFD cell/grid is calculated by

$$J_{cell} = V_d C_{cell}\rho_{cell}A_{cell} \quad (5)$$

The deposition flux is assumed to be one-dimensional and constant in the concentration boundary layer, and the particle diffusivity equals the turbulence viscosity. The dimensionless deposition velocity can be evaluated differently based on the surface orientations [34]:

$$V_d = \begin{cases} \frac{V_s}{1-e^{-V_s I}}(upward) \\ \frac{V_s}{e^{-V_s I}-1}(downward) \\ \frac{u^*}{I}(vertical) \end{cases} \quad (6)$$

Where $u^* = \sqrt{\frac{\tau_W}{\rho}}$; *I* is an integral factor with the details available in the literature [34].

2.2 Validations

- Ceiling fan model validation

In this study, the commercial CFD software tool, ANSYS FLUENT [35], is used, and the moving reference frame (MRF) [35] is used to model the fan rotation. A comprehensive experimental study on ceiling fan performance (Fig. 1a) by Raftery et al. [10] is employed for the MRF model validation (Fig. 1b). The ceiling fan with a diameter of 1.5 m (4.9 ft) is mounted at the height of 2.2 m (7.2 ft) in the center of a square room with the size of 6.1 m × 6.1 m × 3 m (20 ft × 20 ft × 9.8 ft) (L × W × H). Two fan blowing directions were considered: fan upward-blowing and downward-blowing, both at 200 rpm. Figs. 1c and 1d show the velocity vectors at the center plane for the downward-blowing (Fig. 1c) and the upward-blowing (Fig. 1d). Fig. 2 compares the measured omnidirectional air velocities and the CFD results at different locations and elevations.

The simulation results generally agree well with the measurements, so the ceiling fan's MRF model is considered valid.

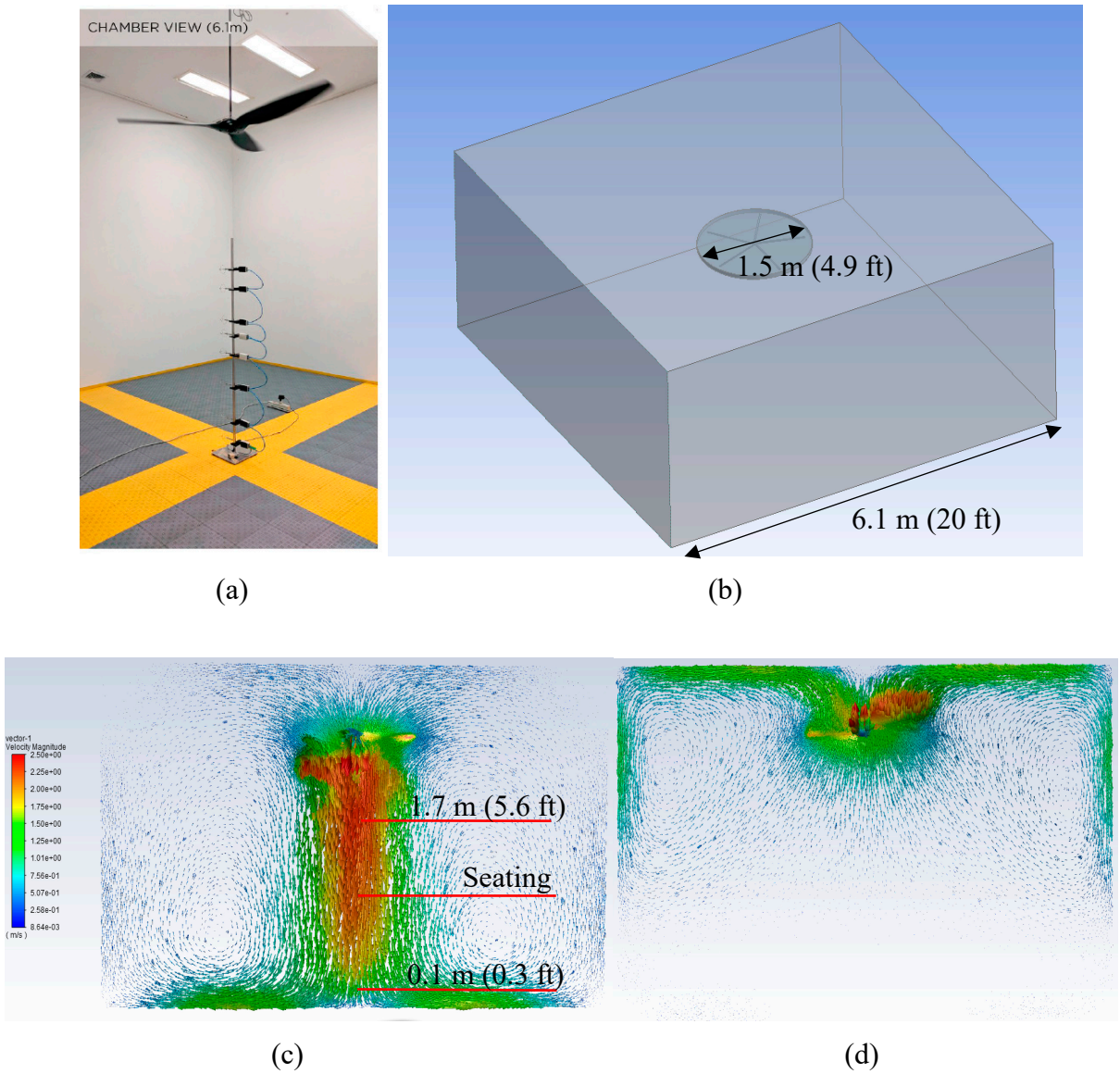

Figure 1. (a) Experimental setup; (b) CFD room model; c) Velocity fields colored by velocity magnitudes at the center plane for (c) the fan downward blowing and (d) fan blowing upwards.

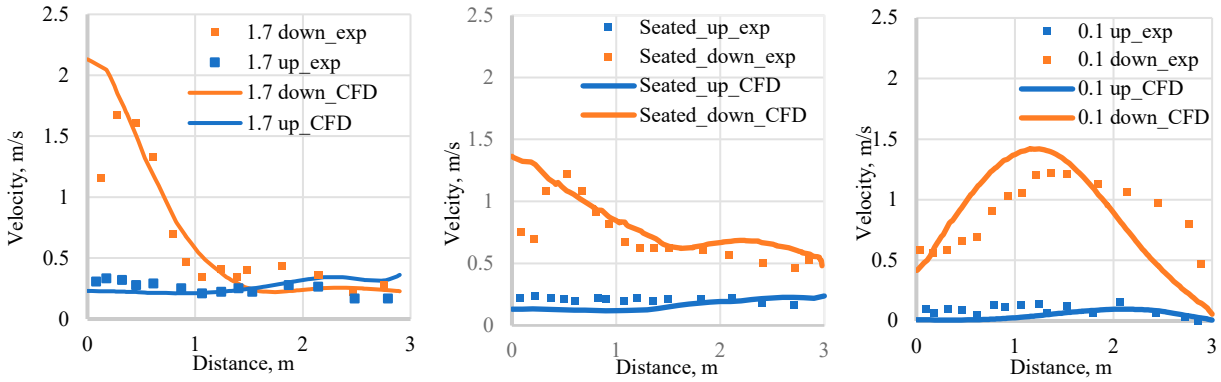

Figure 2. Comparison of the calculated and measured velocities at three planes: 1.7 m (5.6 ft) (left), seating plane (middle), and 0.1 m (0.3 ft) (right) from the floor.

- Drift-flux model validation

The validation of the Drift-flux model is based on the previous chamber study by Zhang and Chen [36] and Gao and Niu [23]. A series of measurements with mono-dispersed 10 μm particles with a density of 1400 kg/m3 (87.4 lb/ft3) released from the inlet was conducted in a room with one outlet shown in Fig. 3. The initial inlet supply velocity is 0.225 m/s (0.738 ft/s). Fig. 3 compares the vertical concentration profiles at three locations: x = 0.2 m (0.66 ft); x = 0.4 m (1.3 ft); x = 0.6 m (2.0 ft). The location x = 0.2 m (0.66 ft) has the highest concentration since it is closest to the particle release. Compared to the previous CFD study by Gao and Niu [23] and the original measurements, the CFD results are close to the measured data, so the Drift-flux model is validated.

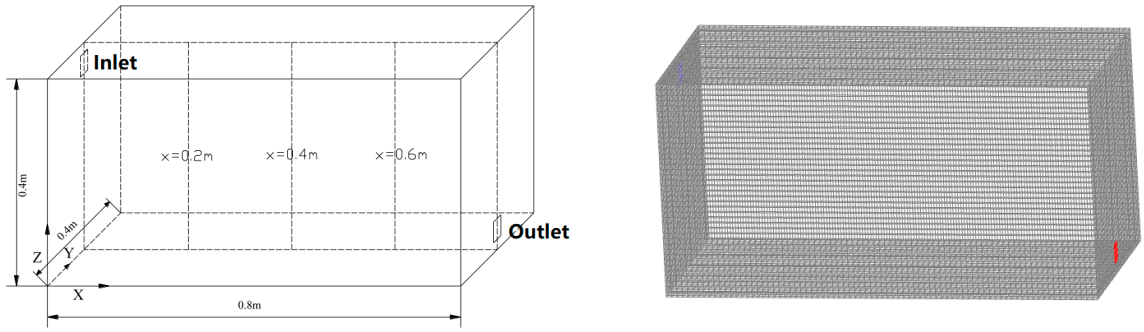

(a) (b)

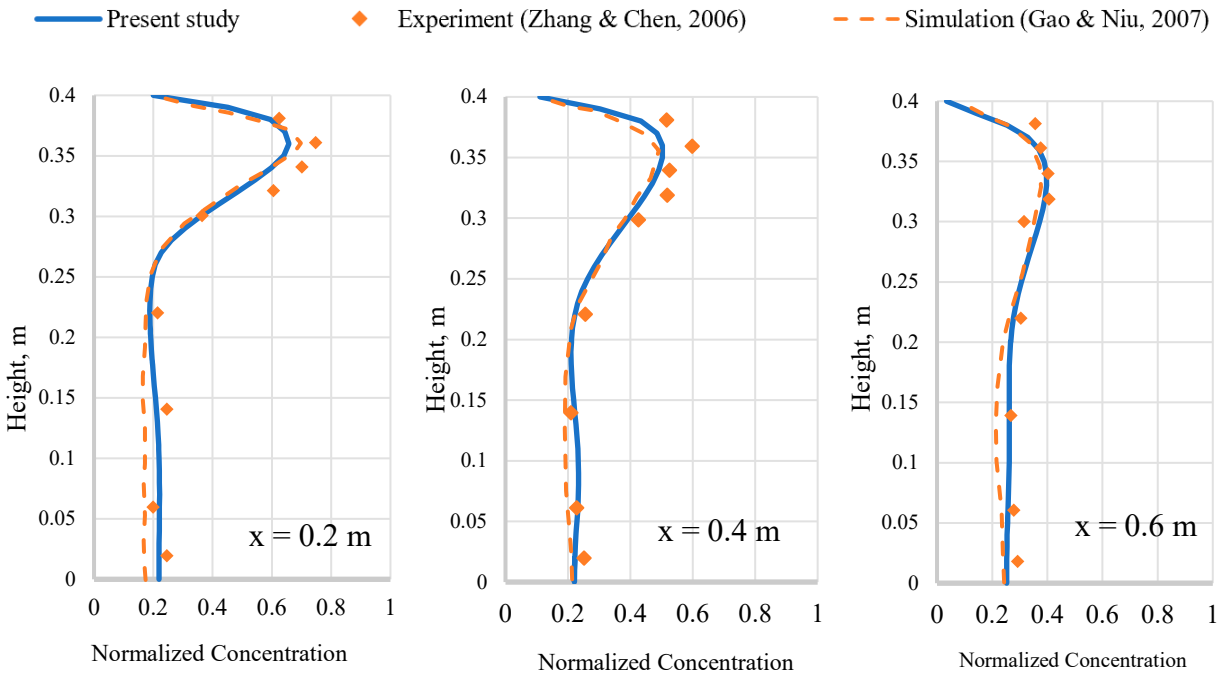

(c)

Figure 3. (a) Chamber setup; (b) CFD chamber model; and (c) comparison of normalized particle concentrations between the measurement and the simulations at (a) x = 0.2 m (0.66 ft), (b) x = 0.4 m (1.3 ft), and (c) x = 0.6 m (2.0 ft).

2.3 Model setup - warehouse model

The industrial warehouse is based on the US DOE warehouse reference building model (Fig. 4a) with a size of 100 m × 46 m × 8.5 m (330 ft × 150 ft × 28 ft) (L × W × H) with two 6.1 m (20 ft) LDCFs (Fig. 4b). The building includes Bulk Storage (Fig. 4b) and Office and Fine Storage. The two LDCFs are in the Bulk Storage, which is only modeled in this study. A warehouse may also include storage racks, which have been modeled previously by porous media models [37–39]. Nelson [40] developed a server rack porous media, and Ambaw [41] modeled a fruit box as the porous media. They indicated that the porosity and resistance of the porous media in three dimensions are essential. Based on these previous studies, this research simulated the warehouse racks by the porous media model (Fig. 4c) with the porosity and flow resistance settings from the literature. The simulation results are reported mostly at two planes of interest: the whole warehouse Breathing Zone (hereafter as "BZ") plane (Fig. 4d), and the vertical plane (Fig. 4e) crossing the two LDCF centers (Fig. 4e), and inside the working zone (hereafter as "WZ") (Fig. 4f). The details of the case setup can be found in Table 1.

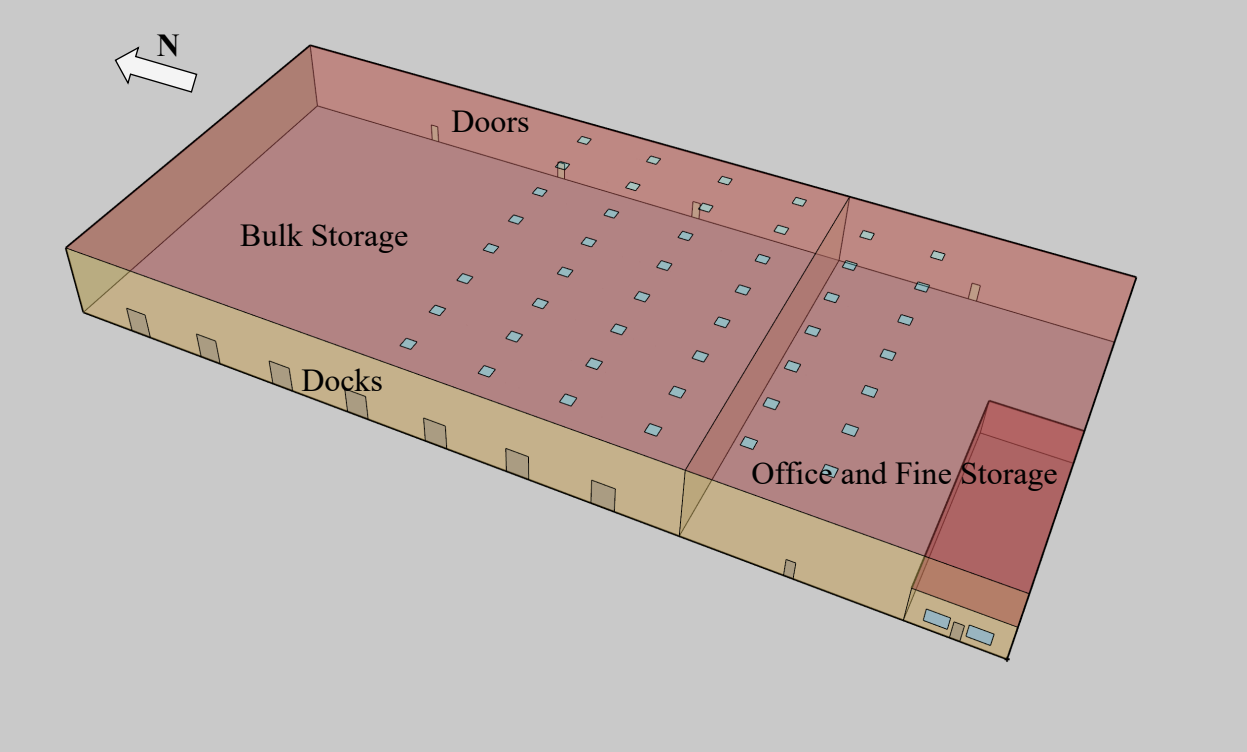

(a)

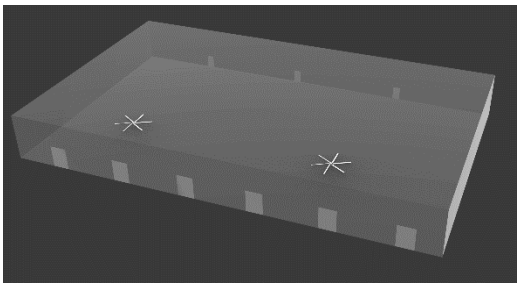

(b)

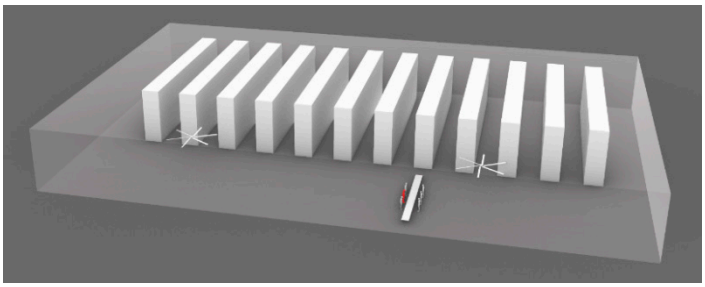

(c)

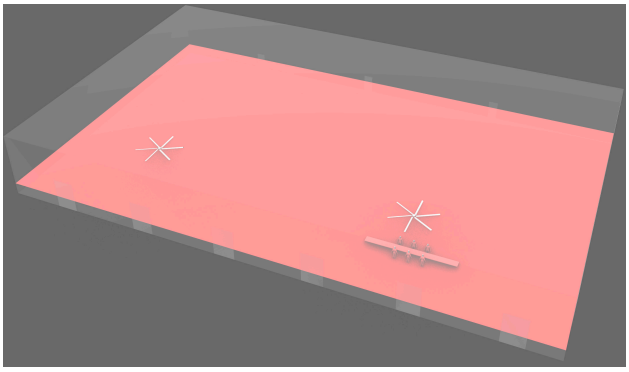

(d)

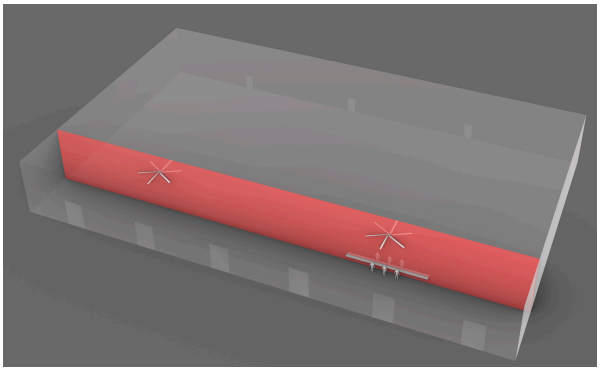

(e)

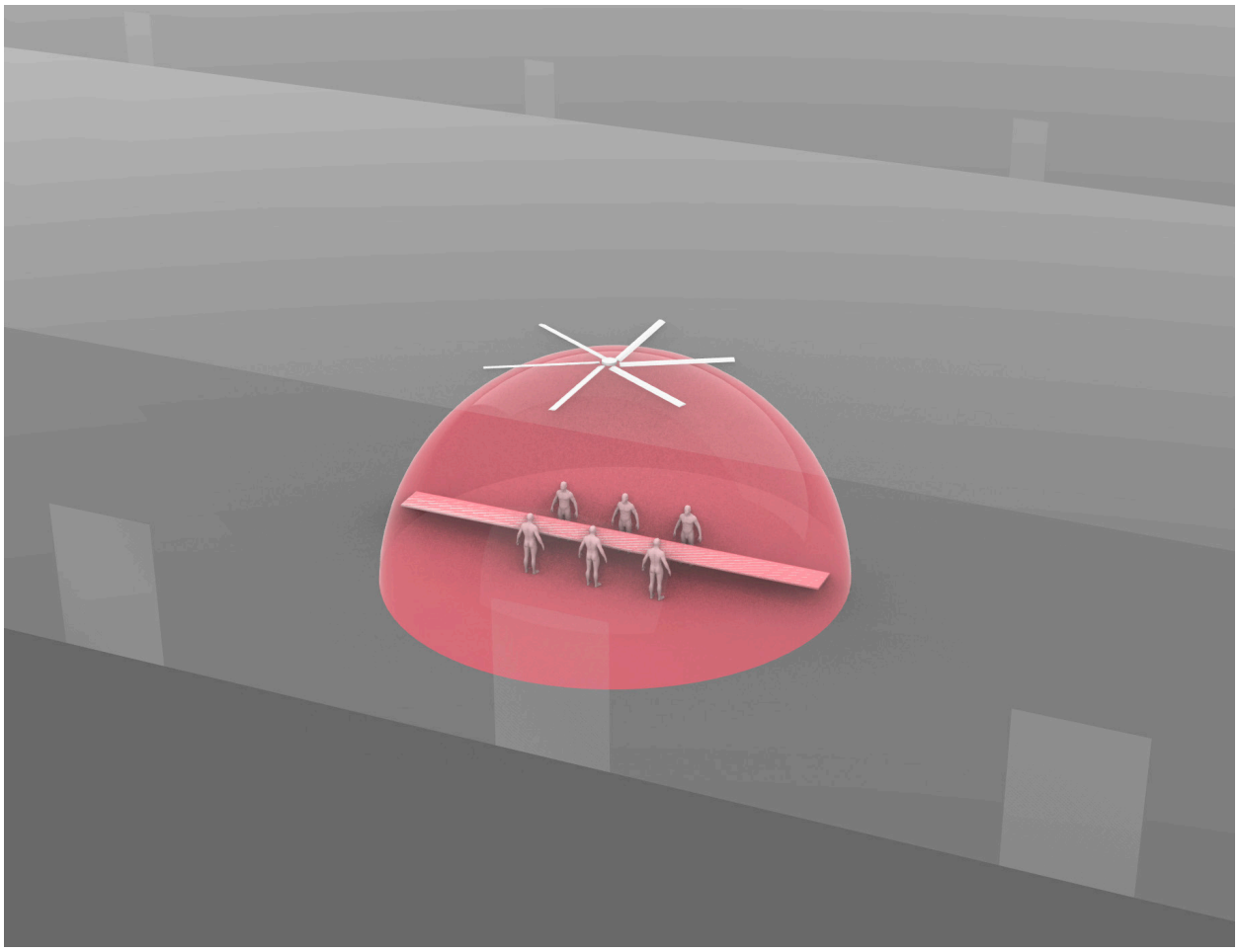

(f)

Figure 4. (a) The DOE warehouse reference building model; (b) The CFD Bulk Storage model with two LDCFs; (c) The CFD model with racks; (d). The whole warehouse Breathing Zone (BZ) plane; (e) The vertical plane; and (f) the Working Zone (WZ) with workers of interest.

- Particle generation distribution

Based on the literation review [19], the particle size for loud speaking (shouting) can be separated into five bins: 0.5 µm, 1 µm, 3 µm, 5 µm, and 10 µm. Fig. 5 shows the particle size profiles with Table 2 for the details of the bin selections. The total particle release rate is 40 particles/s, with most particles sized at 3 µm and over half of the particles less than 3 µm. The particle number generation for 3 µm is 23.31 particles/s.

Table 1. Key CFD model parameters.

Key Parameters	Settings
Mouth opening area	227 mm^2 (0.35 in^2); 17 mm (0.67 in) diameter circle [42,43]
Exhale velocity	3.4 m/s (11.2 ft/s) (loud speaking/shouting) [44]
Exhale temperature	34 °C (93.2 °F) [45]
Number of infectors	One infector at different locations
Infector location	Case dependent – see Fig. 7
Particle diameter	Particle bins (0.5 µm, 1µm, 3 µm, 5 µm, 10 µm)
Particle surface deposition	Particle sinks by UDF [23]
Airborne decay rate	No measurable decay rate [46]
LDCF rotating speed	78 rpm (100% speed); 16 rpm (20% speed); no fan running
LDCF maximum volume flow rate	Q= 90 m^3/s (192,000 CFM) at 78 rpm from AMCA
Fan diameter	6.1 m (20 ft)
Fan locations	Two fans 36.6 m (120 ft) apart; 7.6 m (25 ft) from the south wall; 18.3 m (60 ft) from the west wall surfaces; 2.1 m (7 ft) under the ceiling
Outdoor dry bulb temperature	Summer 32 °C (89.6 °F) and Winter -17.5 °C (0.5 °F) [47]
Body temperature	33 °C (91.4 °F) [44]
Surface temperatures	From EnergyPlus simulation (see Fig. 6)
Inlet ventilation rate	0.37 m^3/s (780 CFM) per dock
Steady or Transient	See simulation scenarios
Turbulence model	Standard k-ε [48]
Species transient timestep	Adaptive 0.1s to 60 s
Mesh size near the fan	10 mm (0.39 in)
Mesh size near the mouth	2 mm (0.08 in)
Rack geometry	24 m × 6 m × 2.4 m (80 ft × 20 ft × 8 ft)
Packing line	12 m × 0.9 m × 0.1 m (40 ft ×3 ft × 0.3 ft)
Fan speed type	3 (7 additional speeds for selected case - U-H-D-3)
Reverse fan speed	2
Total simulations	223
Total mesh grids/case	14.6 million
Computing time/case	6 hrs (steady-state airflow only); 8 hrs (transient Drift-flux)

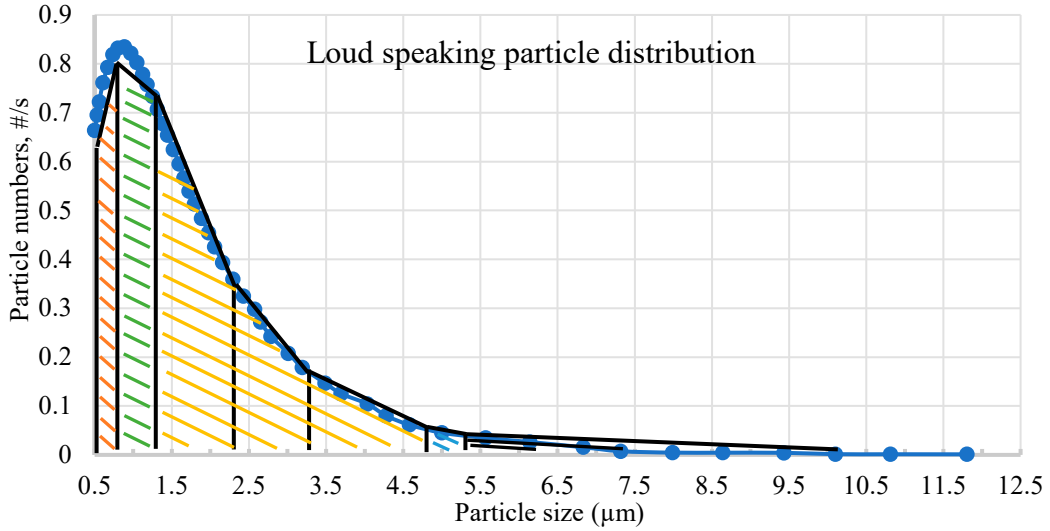

Figure 5. Particle distribution for loud speaking/shouting.

Table 2 Particle concentration distributions for selected bins.

Particle size bin (μm)	0.5~0.75	0.75~1.25	1.25~4.75	4.75~5.25	5.25~10
Bin width (μm)	0.25	0.5	3.5	0.5	4.75
Particle generation (#/s)	4.47	9.33	23.31	0.54	2.35
Particle number fraction	11.17%	23.34%	58.27%	1.36%	5.87%
Mass generation (kg/s)	2.92E-16	4.89E-15	3.29E-13	3.55E-14	1.23E-12
Mass generation (lb/s)	6.44E-16	1.08E-14	7.25E-13	7.83E-14	2.71E-12
Mass fraction	0.02%	0.31%	20.59%	2.22%	76.87%

- Wall thermal boundary conditions

The warehouse is assumed to be located in Chicago, IL, USA. The design day is July 21 for summer and January 21 for winter. The wall thermal boundary conditions were obtained from the EnergyPlus simulation of the DOE warehouse for the design days (Fig. 6). Note that the study focuses on the summer scenario, and a few simulations are conducted for a selected case under the winter conditions. When the warehouse is open from 8 AM to 5 PM on the summer design day, the average temperature is 27.6 °C (81.7 °F) for all the walls, 29.5 °C (85.1 °F) for the roof, and 26.2 °C (79.2 °F) for the floor. For the winter conditions, 11.6 °C (52.9 °F) for the walls, 10.4 °C (50.7 °F) for the roof, and 11.2 °C (52.2 °F) for the floor and -17.5 °C (0.5 °F) for the outdoor air temperature.

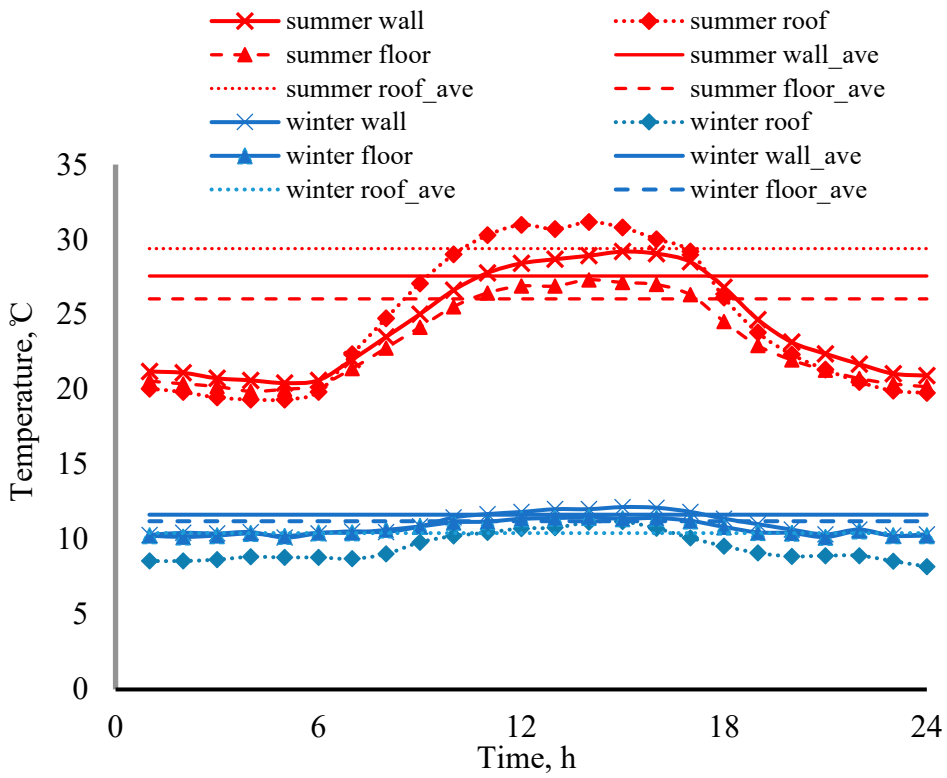

Figure 6. Warehouse surface temperatures from EnergyPlus simulation.

2.4 Simulation assumptions

It is important to address the underlying assumptions of the simulations before any results are reported. Here is a list of the assumptions in the current study.

- This study modeled the particle droplets generated from an infector and their distributions in the warehouse. The actual absolute values of COVID-19 infection risks are not the focus of this study. Therefore, all the results, the conclusions, and the associated guidelines should be interpreted on a relative basis.
- This study considers the particle release from loud speaking and does not consider other respiratory scenarios.
- This study is based on the Drift-flux model with limitations in interpreting particle-air and particle-particle interactions. For example, a particle is with one-way coupling with the airflow, and no particle accumulation, coagulation, resuspension are modeled, although the gravitational and surface depositions have been addressed.
- Therefore, any other assumptions associated with the Drift-flux model also apply. For example, all the particles are spherical with constant density and diameter; the model does not consider natural particle decay or any virus-related biological decay behavior, so the particle concentrations could be overestimated.
- The effects of occupant and warehouse vehicle movements on the airflow are not considered, although the airborne particle transmission is modeled for an 8-hour transient process. In addition,

the thermal plume from an occupant is considered stably established. So, the thermal plume in this study could be overestimated, and horizontal particle spreading could be underestimated.

- The fan operation does not affect the ventilation rates through docks and doors in the simulations, and the internal surface temperatures are assumed constant. In reality, fan operation may likely increase or reduce ventilation airflows through openings in the building envelope compared to a scenario without a fan operating.
- The particle deposition to porous rack surfaces is not considered so that the spatial particle concentrations could be overestimated for cases with racks.
- The fan is assumed to be constantly running, so intermittent operation or dynamic speed changes are not considered.

2.5 Simulation scenarios and case coding

The parametric study includes different locations and arrangements of the packing line relative to the ceiling fans and the worker locations. Note that in all cases, the packing line is placed near the right-side fan, the center of which is thus used as the reference for the "**L**eft" or "**U**nder" location, meaning the packing line is to the left or "under" of the right-side fan.

- The location of the packing line is coded relative to the center of the right-side ceiling fan as:
  - **M**iddle (**M**, 18.3 m (60 ft)) – the middle of the two fans;
  - **L**eft (**L**, 9.1 m (30 ft)) – the left to the right-side fan;
  - **U**nder (**U**, 0 ft) – directly under the right-side fan.
- The orientation of the packing line is coded as:
  - **V**ertical (**V**) – vertically placed (E-W direction) or
  - **H**orizontal (**H**) – placed horizontally (N-S direction).
- The worker arrangement is coded as:
  - **D**ouble row (**D**) – all workers standing in two lines, or
  - **S**ingle row (**S**) – all on a single side.
- The worker distance is coded as:
  - **3** ft (0.9 m) (**3**) – 3 ft apart, or
  - **6** ft (1.8 m) (**6**) – 6 ft apart.
- Fan speeds and blowing directions are coded as:
  - **F**an **S**peed with **3** m/s (~ 10 ft/s) (as defined by Eq. 7): **FS-3** = 100% (78 rpm);
  - **F**an **S**peed with **0.6** m/s (~ 2.0 ft/s): **FS-0.6** = 20% fan speed (16 rpm);
  - **F**an **S**peed with 0 m/s: **FS-0** = fan off (0 rpm).
  - Fan blowing air downwards, by default, unless indicated as "**reverse**" for fan blowing air upward.
- Cases with heat transfer/energy equation disabled (no thermal buoyancy) indicated as "**noheat**"
- Cases with racks indicated as "**racks**"
- Results for average particle concentration at the whole-warehouse **B**reathing **Z**one indicated as "**BZ**"
- Results for average particle concentration at the **W**orking **Z**one indicated as "**WZ**"

The "fan air speed" [10] is defined by:

$$FS = \frac{Q}{\pi D^2/4} \quad (7)$$

Where

Q = fan flow rate, m^3/s (CFM)

D = fan diameter, m (ft)

For example, $FS\text{-}3 = \frac{192000}{\pi \cdot 20^2/4} \approx 3\ m/s\ (10\ ft/s)$; $FS\text{-}0.6 \approx 0.6\ m/s\ (2\ ft/s)$.

The coding convention is shown in Fig. 7. For example, the case of U-H-D-3 means that the packing line is horizontally placed and directly under the fan with double rows of workers standing 3 ft (0.9 m) apart.

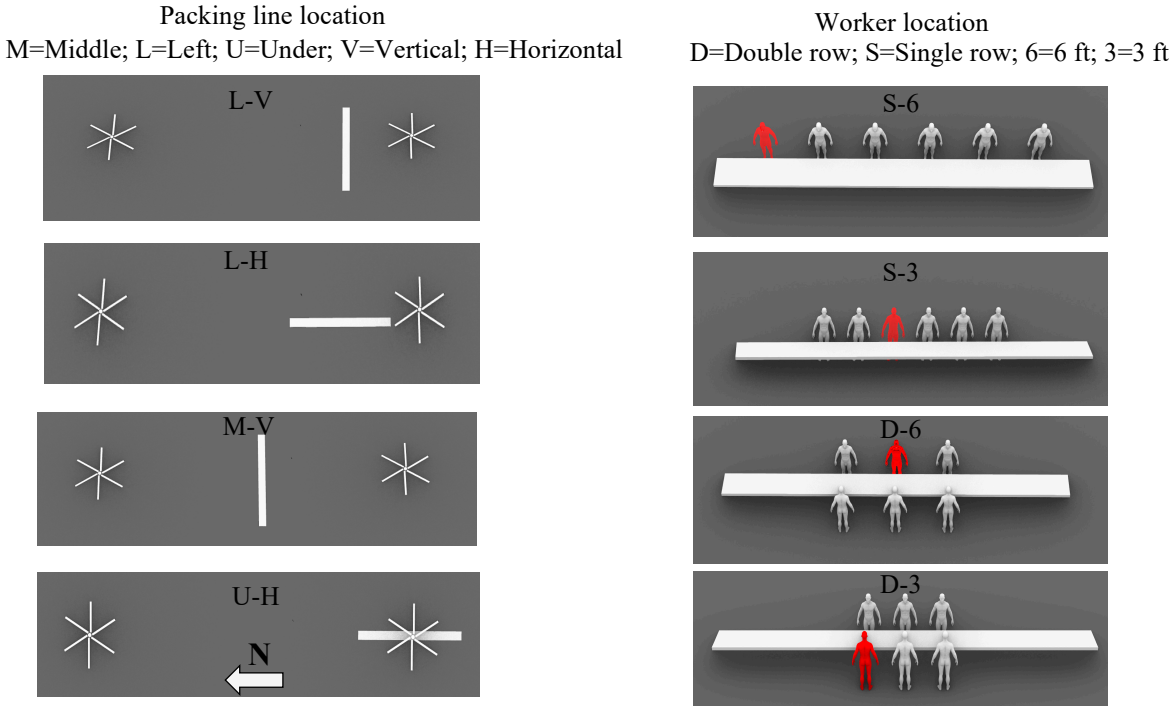

Figure 7. Parametric case scenarios and their coding conventions (the person colored by red is the infector).

3. RESULTS

3.1 Steady-state airflow distributions

The steady-state airflow distributions are plotted as the velocity magnitude contours at the BZ plane (the top row) and the vertical plane (the bottom row). Fig. 8 shows a selected case of U-H-D-3 for different fan air speeds, i.e., 3 m/s (10 ft/s) (100% fan speed), 0.6 m/s (2 ft/s) (20% fan speed) and 0 m/s (fan off). When the fan blows air downwards, both FS-3 and FS-0.6 create a high-speed circular region under the fan with a lower speedcore directly under the fan. FS-3 has an airspeed exiting the fan of 3.0 m/s (591 fpm), and most of the whole warehouse seems to be well ventilated, especially in the horizontal plane. When the fan operates at the 20% speed, FS-0.6 shows that most of the region far from the fans at the horizontal breathing zone plane has a low

speed except the regions closer to the fans, indicating FS-0.6 creates less air mixing in the whole warehouse than FS-3. When the fan does not operate in the FS-0 case, most airspeed is less than 0.2 m/s (0.7 ft/s), and the thermal plume creates the major local airflow from the worker group, besides the airflow through open doors and docks. When comparing the summer and winter conditions, a stronger vertical and horizontal mixing (i.e., higher spatial speeds) are observed in the winter than in the summer, especially for FS-0.6 and FS-0, as indicated by generally higher airspeeds in the winter cases near the ceiling. Therefore, the steady-state airflow illustrates how the whole warehouse is ventilated at different fan speeds. Similar trends are also observed for other cases, the details of which can be found in the Appendix.

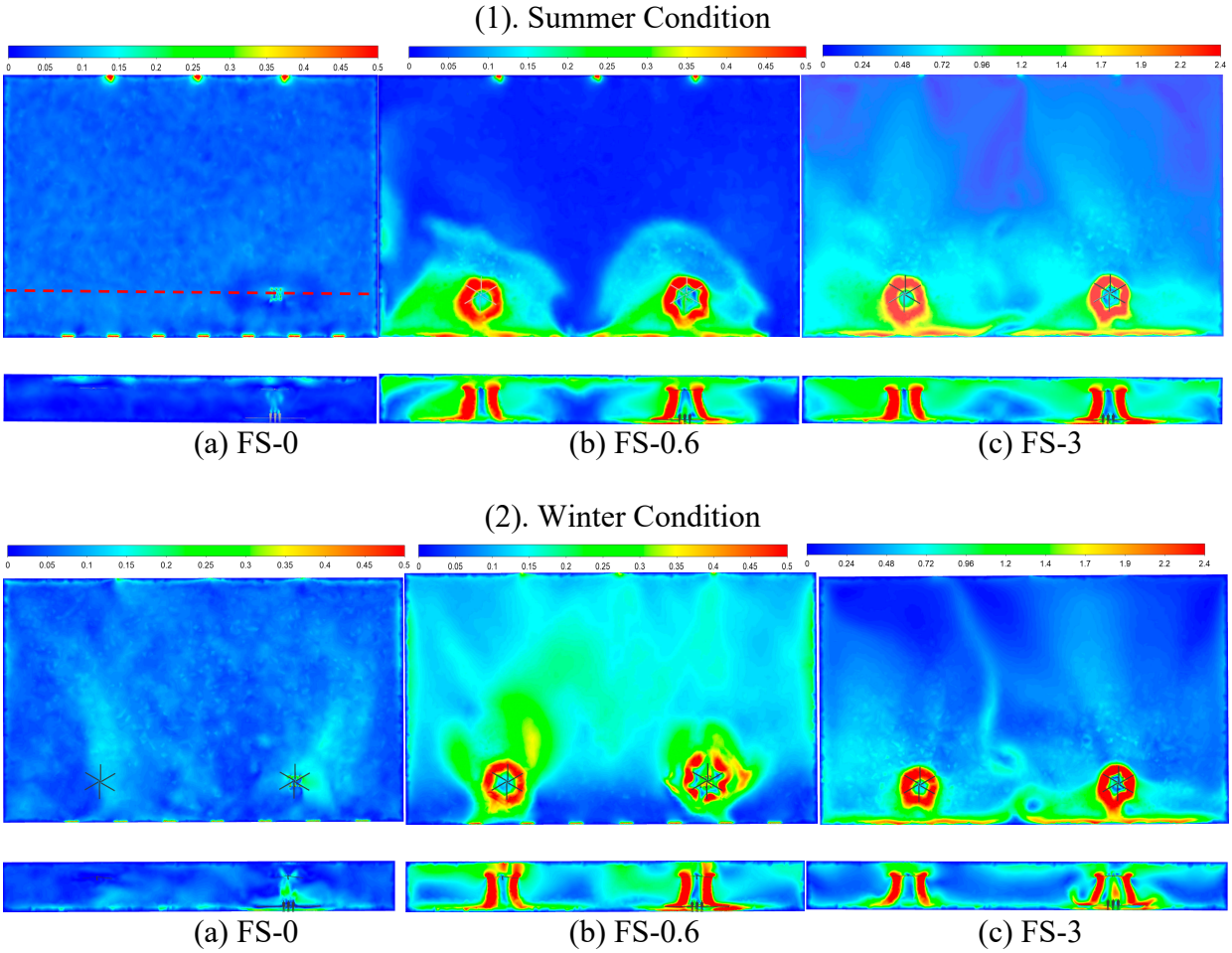

Figure 8. Steady-state distributions of airflow velocity (m/s) for a selected case (U-H-D-3) for three fan speeds (the dashed line is the location of the vertical plane) for (1) the summer condition and (2) the winter condition.

3.2 Transient BZ average particle concentration distributions

Transient simulations of particle dispersions were conducted for eight hours' spreading based on the steady-state airflow. First, all particle bins in Table 2 are simulated for a selected case (See Appendix). It was found that 3 μm is the dominating airborne particle with a representation trend among all particles. So all the rest of the simulations are based on the particle size of 3 μm.

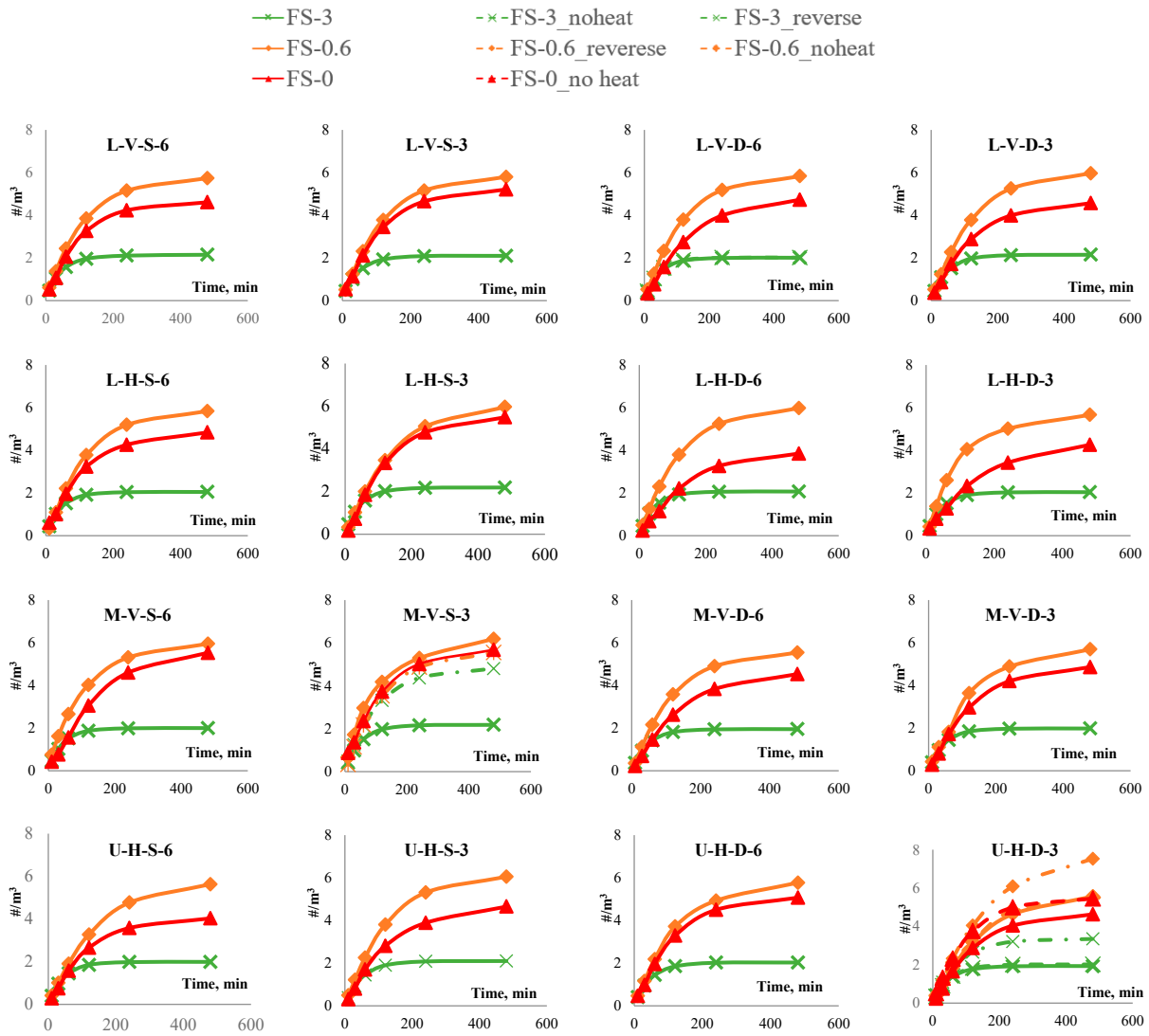

Figure 9. Transient Whole-warehouse Breathing Zone average concentrations (Summer).

Figure 9 compares the spatially averaged particle concentrations obtained from averaging the particle concentrations at all grid cells in the whole warehouse breathing zone (BZ). It is observed that:

- FS-3 (solid green lines) cases achieve the lowest average particle concentrations, FS-0.6 (solid orange lines) have the highest concentrations, and FS-0 (solid red lines) fall between these two cases at the BZ for all cases, except the early stage of releasing (<100 mins).
- The observed trend above can be clearly represented by the results at the end of the 8 hours, so it is possible to focus on the analysis for the end of the 8th hour.
- At the 8-hour point, the lowest concentration among all cases is observed for the case U-H-D-3 with FS-3 (100% fan speed), and the highest concentration for FS-3 is the case L-H-S-3 (i.e., the case with the packing line to the **L**eft of the right-side fan and **H**orizontally/N-S placed with **S**ingle-role workers standing **3** ft apart). Therefore, in later sections, we will focus on the

analysis of the case of U-H-D-3. For example, a few extra cases were conducted to investigate the impacts of the thermal plume ("noheat") and reversed fan blowing direction ("reverse").

- When the fan operates at full speed (FS-3), it takes only around 4 hours to reach the steady-state, whereas the particle concentrations keep increasing at the end of 8 hours for FS-0.6 and FS-0.

3.3 Particle concentration distributions

We plot the concentration contours at the BZ for all cases at the end of the 8th hour in Fig. 10. The results for the winter conditions are included in the Appendix.

- When the fan is off (FS-0), a clear spreading trend from the docks to the doors (visually from the bottom to the top portion in Fig. 10) is observed due to the infiltration flow from the loading docks to the warehouse doors. The particle is unevenly distributed with local "hotspots" and lower concentration regions near warehouse corners and the loading docks.
- When the fan operates at 20% speed (FS-0.6), the particles more uniformly spread across the warehouse with generally higher whole-warehouse concentrations than FS-0.
- When the fan runs at 100% speed (FS-3), the whole-warehouse is well-mixed with the lowest concentration for all cases regardless of the infector and packing line locations, consistent with the previous observations. The last figure of Fig. 10 shows the spatial difference for FS-3 for the max concentration = 2.6 #/m^3. By observation, U-H-D-3 has the lowest concentration, and L-H-S-3 is the highest, consistent with the previous conclusion.

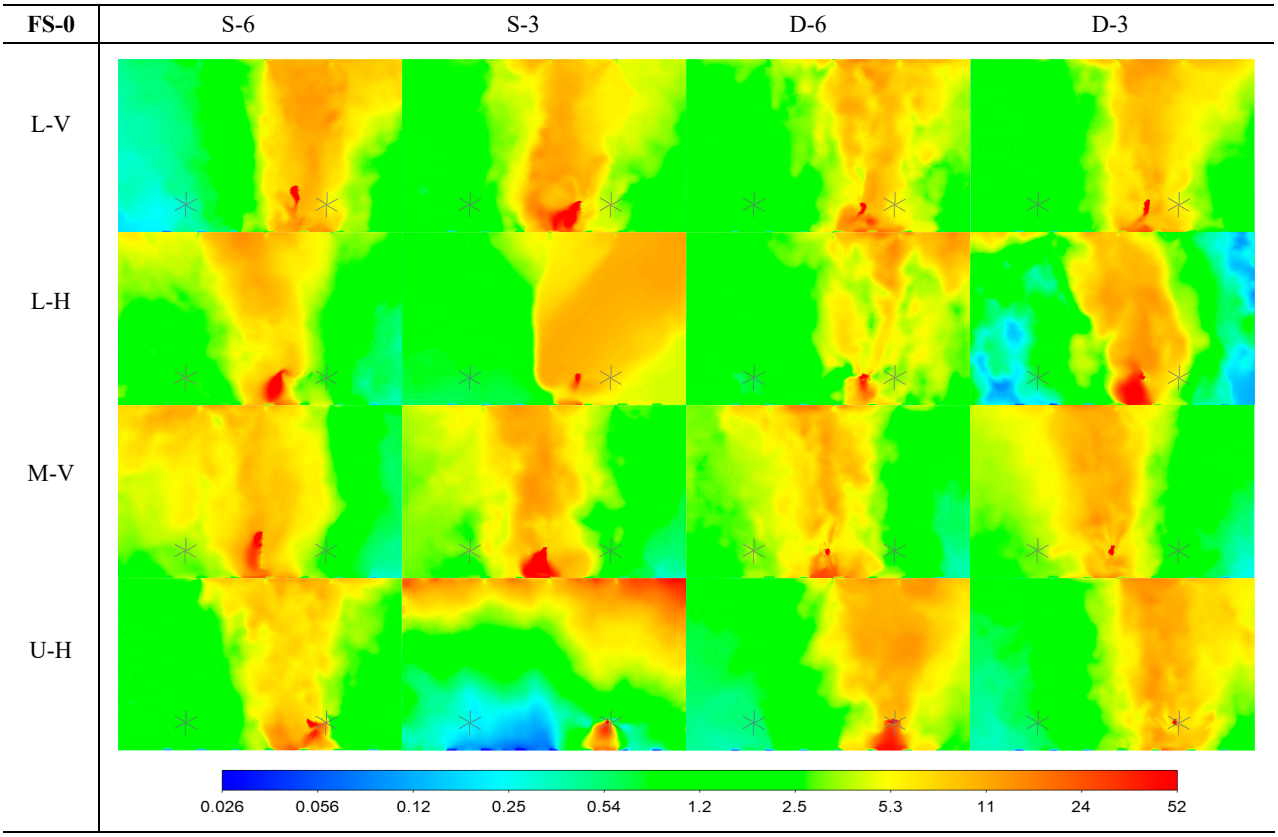

FS-0.6	S-6	S-3	D-6	D-3
L-V	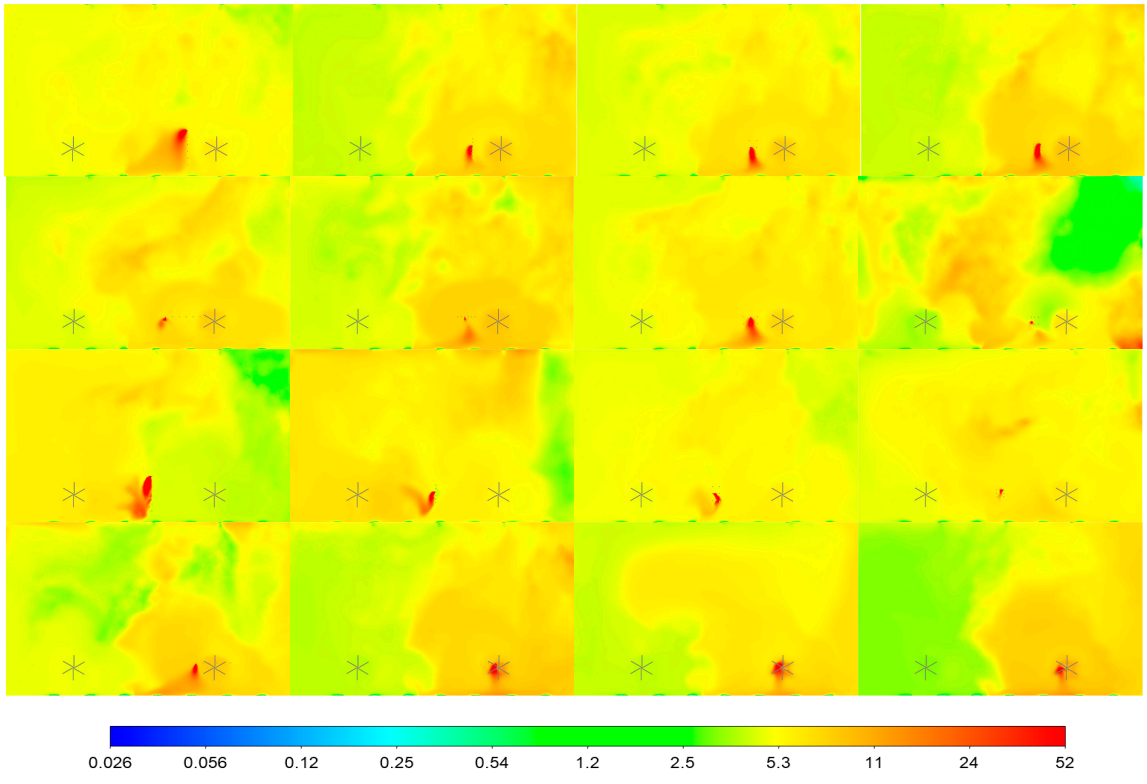			
L-H				
M-V				
U-H				

FS-3	S-6	S-3	D-6	D-3
L-V	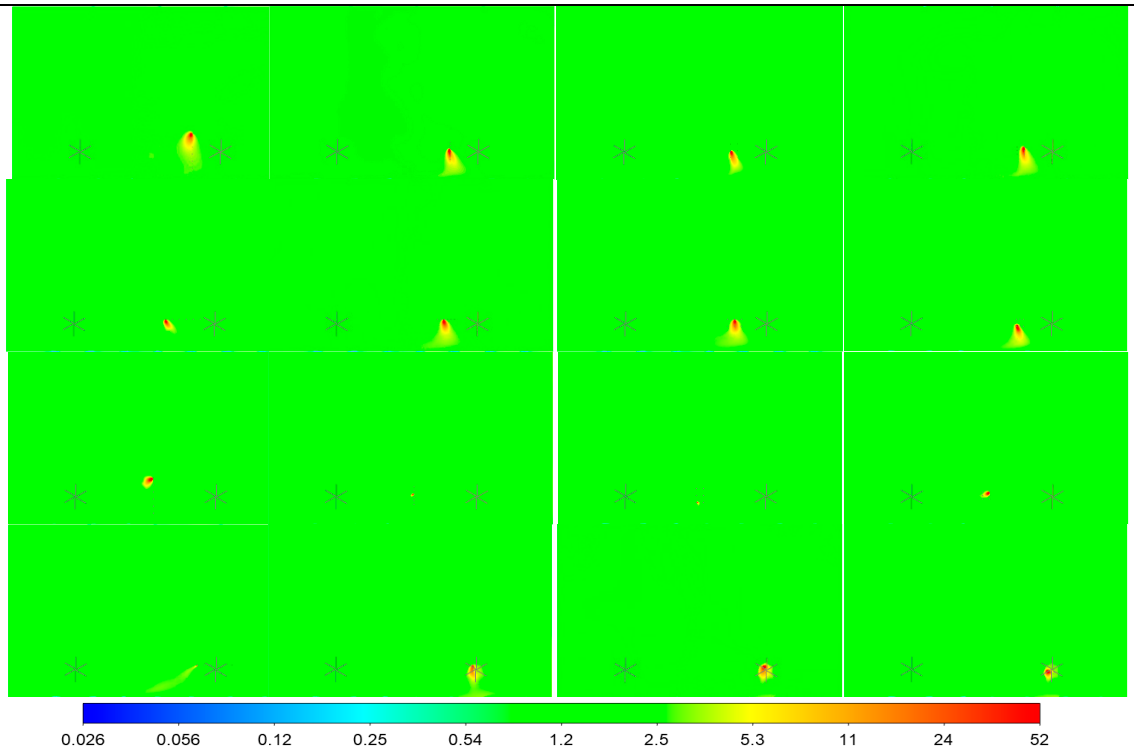			
L-H				
M-V				
U-H				

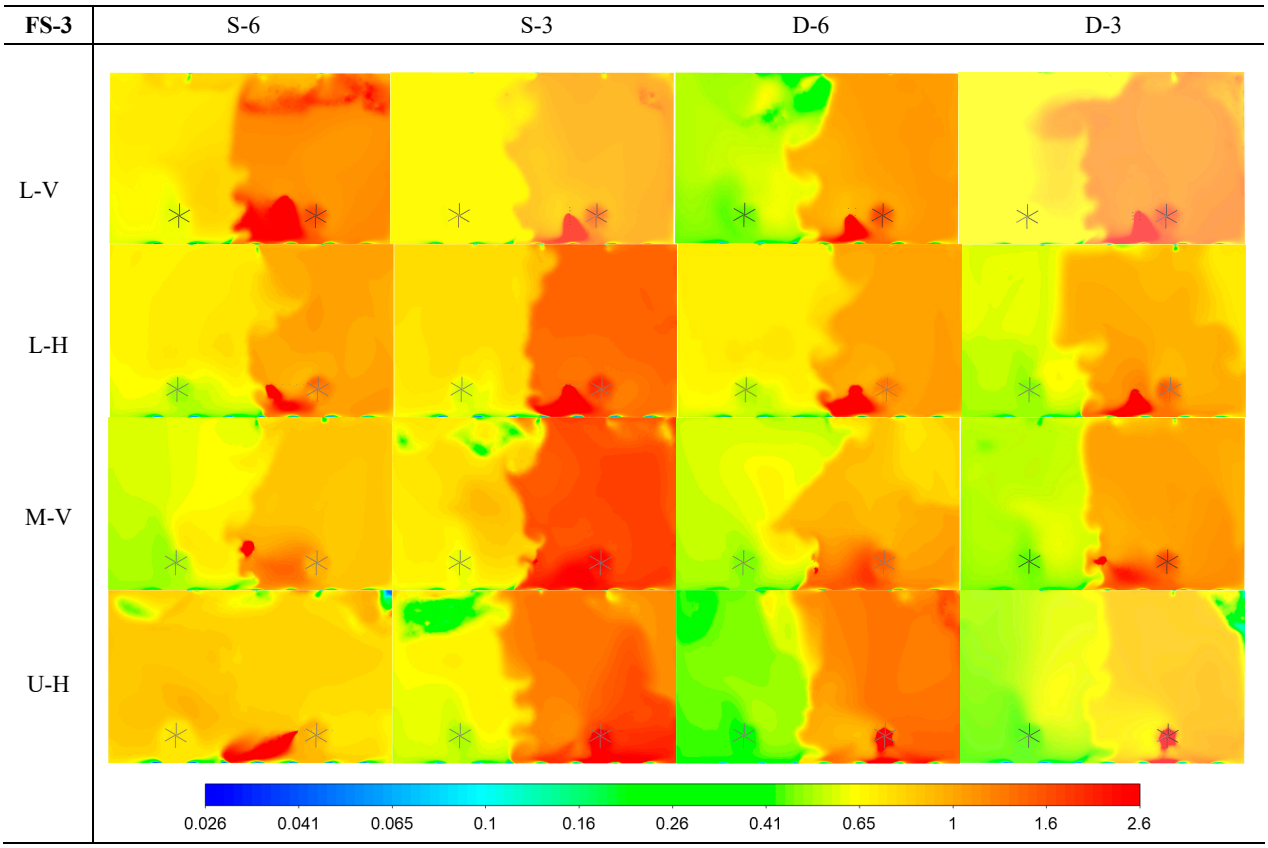

Figure 10. The whole-warehouse Breathing Zone (BZ) concentration contour at the end of the 8th hour for FS-0, FS-0.6, FS-3 (52 #/m^3 max), and FS-3 (2.6 #/m^3 max) (Summer).

3.4 Whole warehouse breathing zone and working zone concentrations

A quantitative comparison of the spatially averaged concentrations at the BZ and the working zone (WZ) is shown in Fig. 11.

- Again, FS-0.6 (solid orange bars) shows the highest BZ concentrations for all cases, and FS-3 (solid green bars) contributes to the best mixing and dilution with the lowest concentration.
- In comparison, the WZ concentration is higher than the BZ for every case, and FS-3 again shows the lowest concentration.
- When the fan does not run, the WZ concentration is higher than when the fan operates at either speed for all but one scenario. Apparently, at the 8th hour, the fan operation helps to reduce the concentration level in the WZ through the dilution to the rest of the warehouse
- For L-V-D-6, three more cases with racks were conducted: the racks result in lower concentrations for all cases, but the difference is significant for the WZ. A more detailed analysis of the rack impacts is discussed in a later section.
- For M-V-S-3, when the fan direction is reversed, the BZ and WZ concentrations of FS-3 both increase because of the lower airflow velocity in the space because of the reversal (note BZ results are solid bars)
- In comparison, FS-0.6 concentrations decrease after reversal, indicating a possible correlation of fan speed to the average spatial concentration, and FS-0.6 seems the worst scenario with the highest concentration.

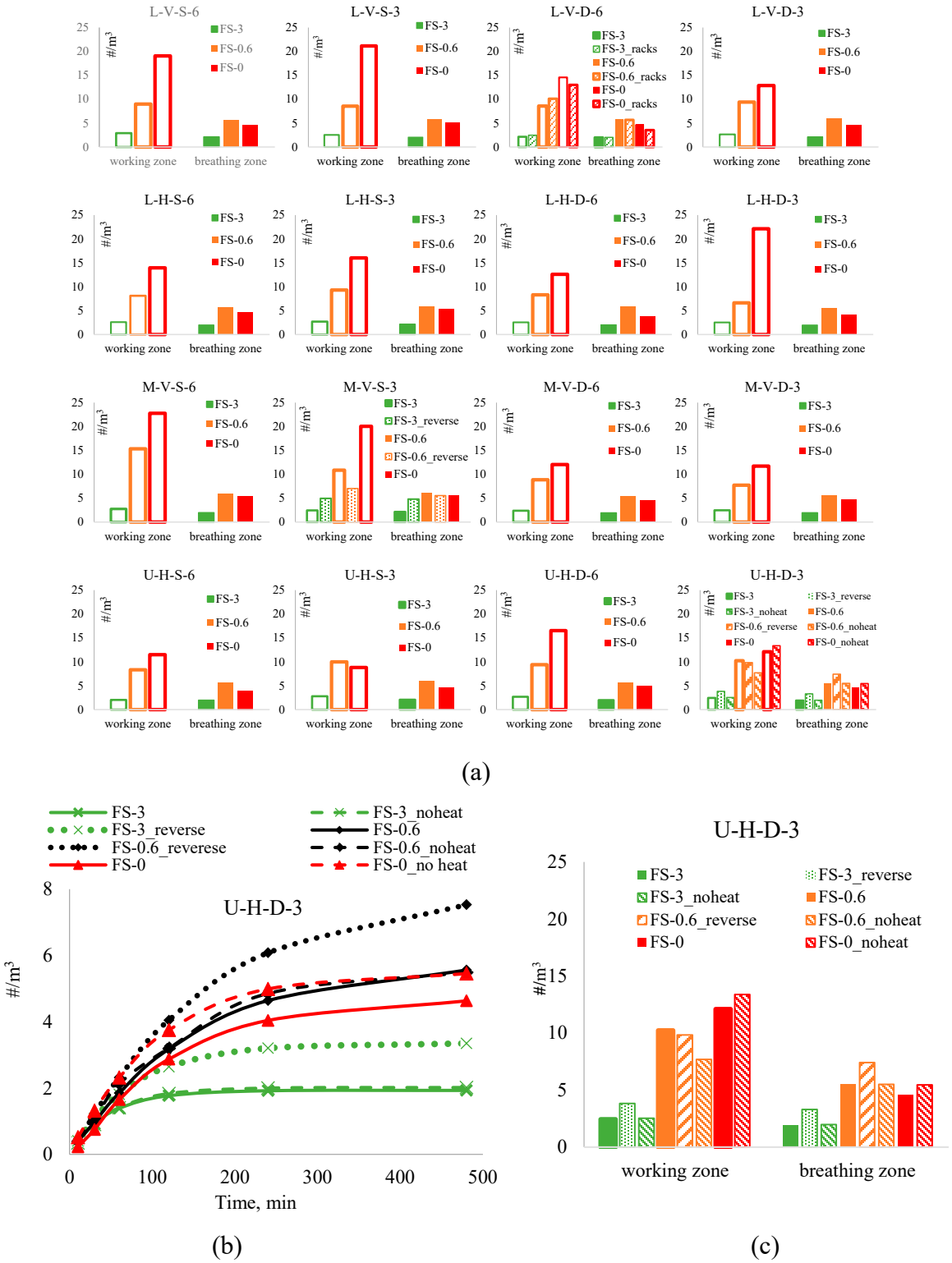

Figure 11. (a) Working Zone and Whole-warehouse Breathing Zone concentrations at the end of 8 hours; (b) transient concentrations; and (c) the concentrations at the 8th hour for U-H-D-3 (Summer).

- For U-H-D-3, similar observations were obtained except that the workers are directly under the fan, so the fan reversal shows different trends for FS-0.6: the BZ concentration increases after the reversal, indicating the reversed fan flow contributes to a better spreading from the WZ to the rest of the warehouse.
- For U-H-D-3, a few simulations (Figs. 11b and 11c) were conducted with the energy balance equation disabled (i.e., "noheat" scenarios) to investigate the impacts from the thermal plumes. It shows that the lack of thermal plumes has minimal impacts on FS-3 due to the fan momentum effect, which essentially dominates the airspeed distribution within the warehouse and fully mixes the air volume.
- The thermal buoyancy clearly affects the FS-0 case, resulting in higher concentrations in both BZ and WZ. The thermal buoyancy force is the primary driving force for the upward motion in FS-0. Without it, the particles become stagnant and maintain a lower portion of the warehouse close to the breathing zones.
- For FS-0.6, the thermal buoyancy force acts in the opposite direction to the fan flow. So, when it is disabled, the fan flow tends to dilute the working zone better to the rest of the warehouse resulting in a lower WZ concentration but slightly higher BZ concentration.
- A closer look at U-H-D-3 in Fig. 11c also confirms the observations. Again, the BZ concentration becomes the highest for the "FS-0.6-reverse" case, indicating that reversing the fan at lower fan speed could significantly increase the whole-warehouse breathing concentration and create a worse scenario.
- On the other hand, for a given fan airspeed, the fan reverse could reduce the space air velocity and thus less surface deposition (Eqs. 5 and 6), and then higher BZ concentration. So, for such a large warehouse, reversing the fan seems not preferred in terms of the whole warehouse breathing zone.

4. DISCUSSIONS

This section discusses the findings for the key parameters, including fan speeds, thermal plumes, surface depositions, working area arrangements, and racks. Although many CFD results are available, it is impractical to discuss all the cases, so a representative case, U-H-D-3, is selected for the analysis.

4.1 Impacts of fan speeds and thermal plume

Figure 12 shows the comparison of the particle concentration for U-H-D-3 to study the impact of fan speeds. Note that the concentration levels are evaluated at the end of the 8^{th}-hour operation for the long-term exposure scenario.

- FS-3 performs the best for both the BZ and WZ.
- FS-0.6 with the reverse operation has the highest particle concentration at the BZ in the summer, and FS-0 is the highest at the WZ in the summer.
- With the fan direction reversed in the summer, the FS-3 performance worsens, and FS-0.6 performs better for the WZ but worse for the BZ.
- In the winter, FS-0 creates the worst situation for both BZ and WZ, so the fan running in the winter helps to reduce the concentration levels in the warehouse. However, reversing the fan in the winter does not necessarily contribute to lower concentration levels in BZ and WZ.
- In the summer, FS-3 with downward airflow always performs the best, so the fan should run at a higher speed.
- The impact of fan speeds is apparently not linear or monotonic.

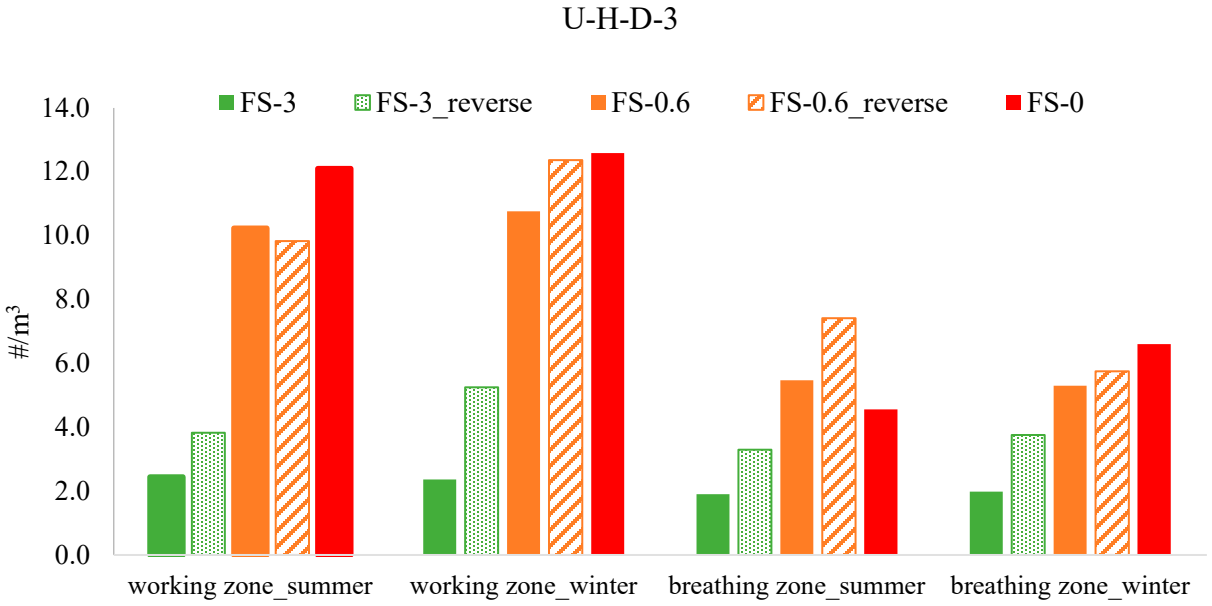

Figure 12. Comparison of fan operations for U-H-D-3 based on the 8th-hour concentration.

To investigate the fan speed impact further, we conducted a series of extra simulations of the fan speeds including 0.9 m/s (3.0 ft/s) (30% fan speed), 1.2 m/s (~4.0 ft/s) (40% fan speed), 1.5 m/s (5.0 ft/s) (50%), 1.8 m/s (6.0 ft/s) (60%), 2.1 m/s (7.0 ft/s) (70%), 2.4 m/s (8.0 ft/s) (80%), and 2.7 m/s (9.0 ft/s) (90%). Fig. 13a shows that:

- For the average whole-warehouse breathing zone concentration, FS-0.6 remains the worst scenario in terms of the highest particle concentration.
- FS-0.9 and FS-1.2 also result in higher concentrations for most of the time than when the fan is off (FS-0), although, for FS > 1.2 m/s (4.0 ft/s), a higher FS contributes to a lower BZ concentration.

If we focus on the concentration at the 8th hour, Fig. 13b illustrates the correlations of the BZ (or BZ) and WZ concentrations (the Y1-axis) and relative reduction with FS-0 as the baseline (the Y2-axis) versus the fan speeds. For the WZ, increasing fan speed always benefits, whereas the fan speed of 0.6 m/s (2 ft/s) (FS-0.6) creates the highest BZ concentration level. Therefore, Fig. 13b provides essential information on how fan speeds impact the BZ and WZ concentrations. Meanwhile, we extracted the "fan zone" (Fig. 13c) velocities in Table 3 to provide the spatial speed values at different fan airspeeds. For example, the maximum air velocity in the fan zone is 4.4 m/s (866 FPM) for the fan operates at full speed of 78 RPM. This corresponds closely with the measured data [10], indicating that the maximum speed below a fan is approximately 1.6 times the fan airspeed. The combination of Fig. 13b and Table 3 provides useful information on spatial airspeed and particle concentration distributions under various fan operations.

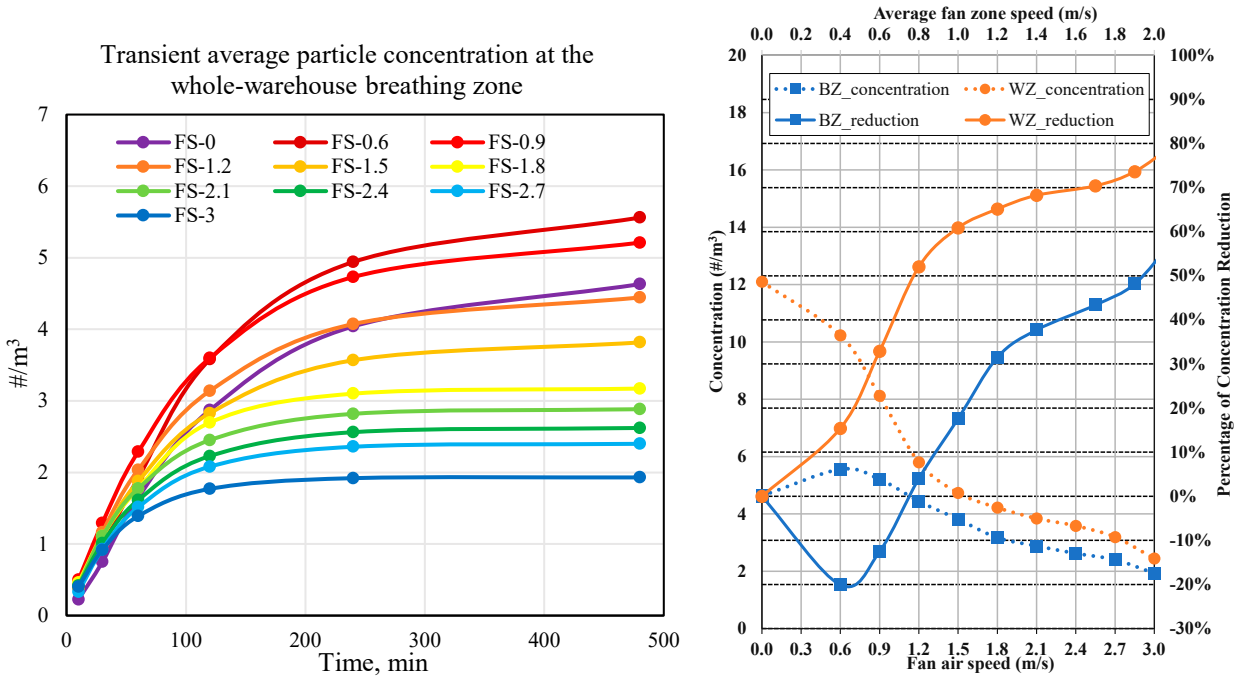

(a) (b)

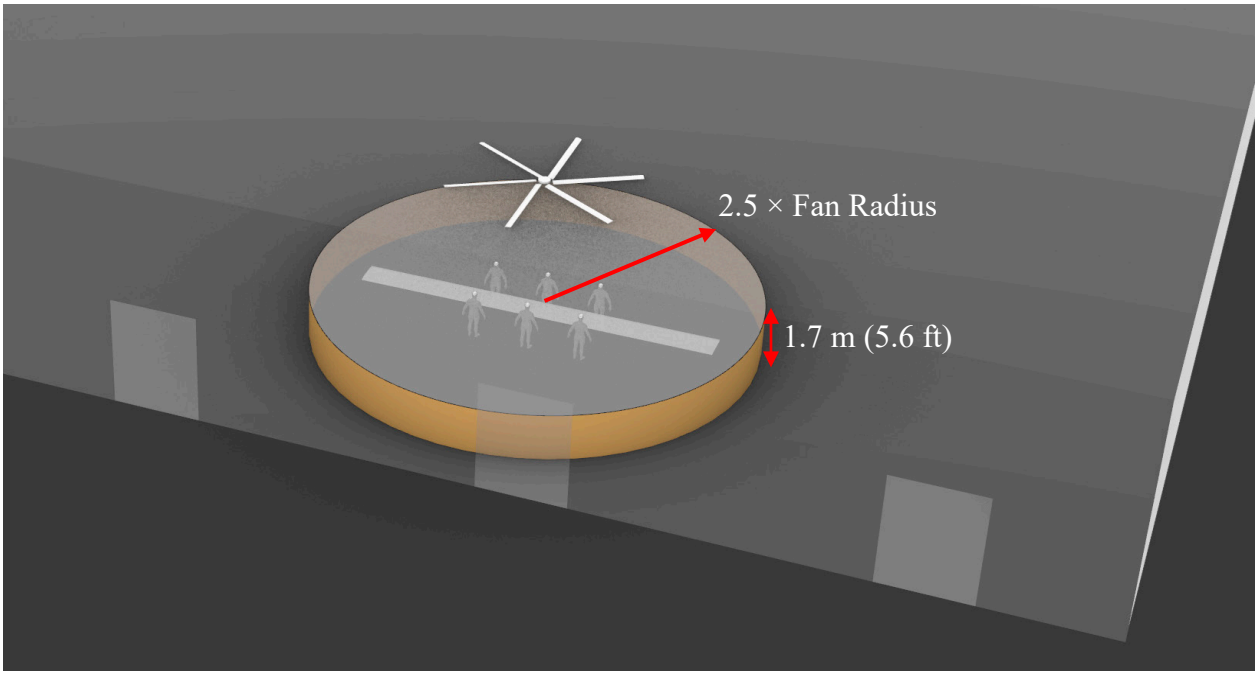

(c)

Figure 13. (a). Transient BZ, and (b) the 8th-hour BZ and WZ concentrations and relative concentration reduction (with FS-0 as the baseline), and (c) the cylindrical shape of "fan zone" (radius = 2.5 × 3.05 m = 7.6 m or 25 ft) for the fan velocity analysis of U-H-D-3 (Summer).

Table 3 Fan air speed and airflow rate data in the fan zone for the case of U-H-D-3.

Fan Speed Label	Fan Speed Percent (%Max RPM)	Fan Speed RPM	Air Speed Leaving Fan(Eq.7) (m/s)[FPM]	Airflow Leaving Fan (m^3/s) [cfm]	Average Air Speed at Side Surface[1] (m/s) [FPM]	Average Fan Zone[2] Air Speed (m/s)[FPM]	Maximum Air Speed in Fan Zone (m/s) [FPM]
FS-0.6	20	16	0.6 [118]	18 [38,400]	0.2 [39]	0.4 [79]	1.0 [197]
FS-0.9	30	23	0.9 [177]	27 [57,600]	0.3 [59]	0.6 [118]	1.3 [256]
FS-1.2	40	31	1.2 [236]	36 [76,800]	0.4 [79]	0.8 [157]	1.7 [335]
FS-1.5	50	39	1.5 [295]	45 [96,000]	0.5 [98]	1.0 [197]	2.2 [433]
FS-1.8	60	47	1.8 [354]	54 [115,200]	0.6 [118]	1.2 [236]	2.5 [492]
FS-2.1	70	55	2.1 [413]	63 [134,400]	0.7 [138]	1.4 [276]	2.9 [571]
FS-2.4	80	62	2.4 [472]	72 [153,600]	0.8 [157]	1.7 [335]	3.4 [669]
FS-2.7	90	70	2.7 [531]	82 [172,800]	0.9 [177]	1.9 [374]	3.8 [748]
FS-3.0	100	78	3.0 [591]	91 [192,000]	1.0 [197]	2.1 [413]	4.4 [866]

[1]"side surface" is the side of the cylinder of the fan zone colored by yellow in Fig. 13c.
[2]"fan zone" is a cylinder around the fan center with a height of 1.7 m (5.6 ft), as shown in Fig. 13c.

To explain why the BZ concentration peaks at about 0.6 m/s (2 ft/s) fan speed in the summer, we selected three horizontal planes, i.e., "Above fan" "Under fan" and "Breathing zone" (the whole warehouse breathing zone), as shown in Fig. 14. Fig. 14 shows that the high-concentration region is lower and narrower in the summer than in the winter. A stronger thermal plume in the winter moves the particles to the higher level of the warehouse near the roof and creates a stronger vertical spreading in both directions.

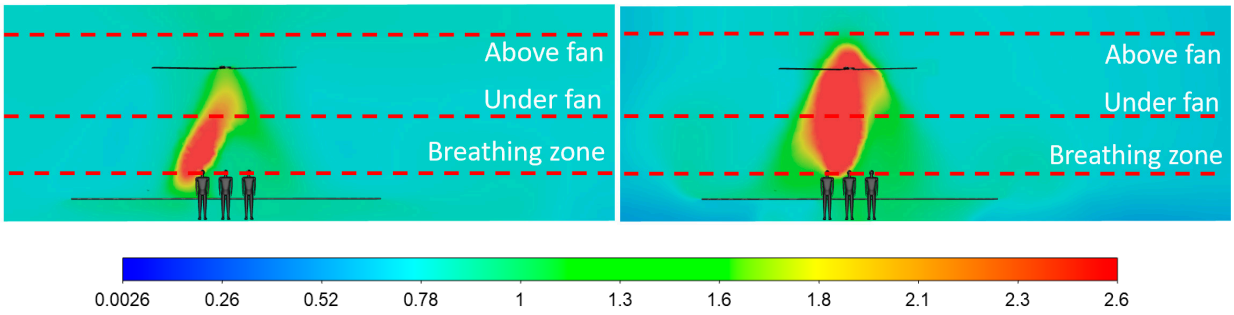

(a) (b)

Figure 14. The selected planes (dashed lines) for the thermal plume study (U-H-D-3, FS-0.6) for the (a) Summer and (b) Winter cases.

Figure 15 extracts the transient average concentrations for the summer case:

- For FS-3, all three zones have the same particle concentrations regardless of the energy equation enabled (by default) or disabled (i.e., "noheat"). So, FS-3 indeed creates a fully mixed zone.
- For FS-0.6, with thermal buoyancy (or the energy equation) enabled, particle stratification develops with the highest concentration at the "Above fan" plane and the lowest at the BZ. When the energy equation is disabled, the vertical distribution is reversed, with the BZ

concentration reaching the highest, which is reasonable because it is closer to the particle source. However, the overall concentrations are higher than when it is disabled. So, the thermal plume dilutes the particle to the warehouse higher level.

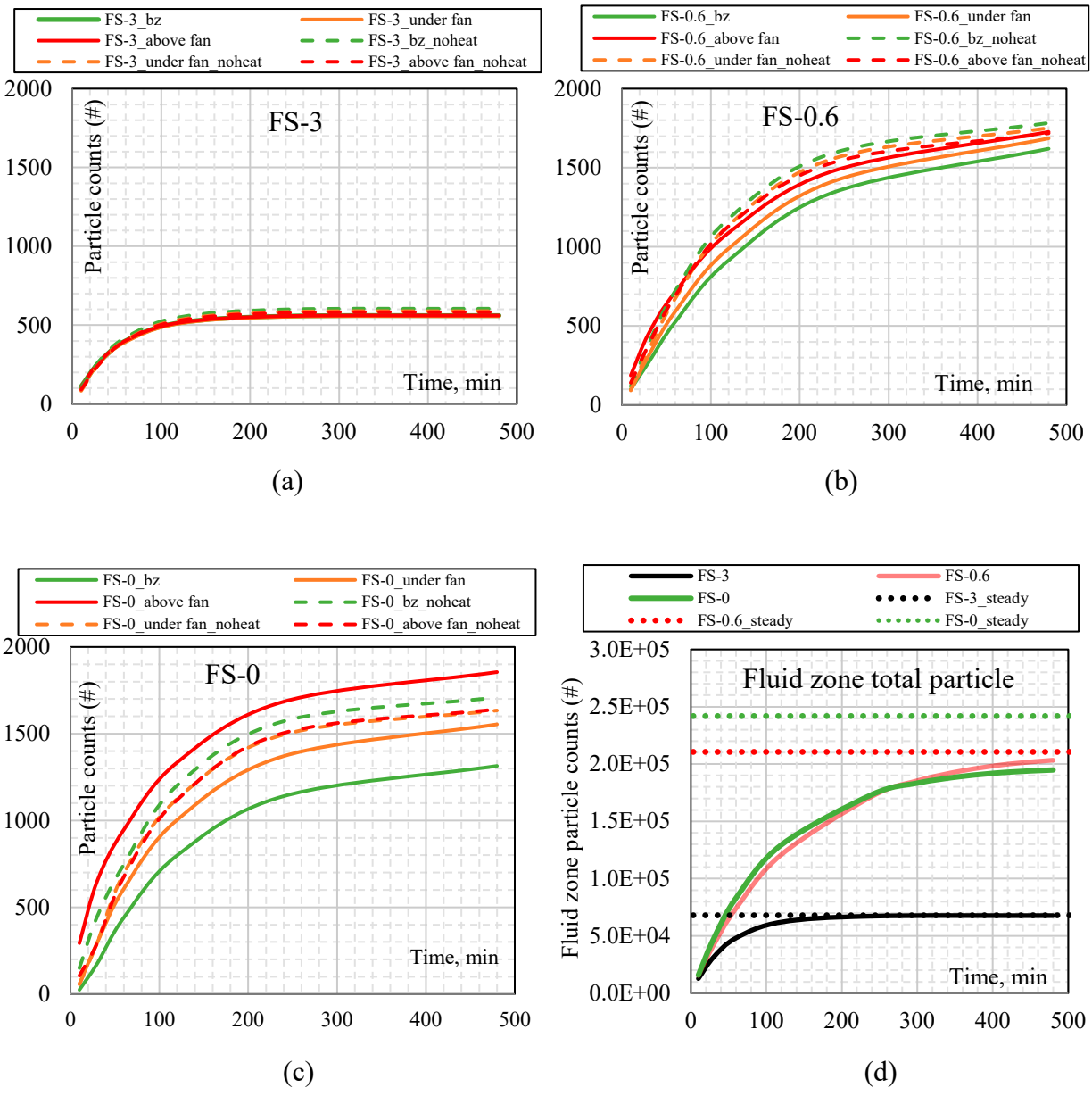

Figure 15. Transient BZ particle counts (#) for (a) FS-3; (b) FS-0.6; (c) FS-0; and (d) Fluid zone total particle counts for all three cases of U-H-D-3 (Summer).

- For FS-0, since the thermal plume primarily drives the flow, the most substantial stratification exists with the highest concentration at the top portion of the space. However, when the energy equation is disabled, the stratification is significantly reduced. This is one of the reasons why the BZ concentration is higher for FS-0.6 than FS-0: thermal plume tends to elevate the particle to the higher level against the fan downflow direction, so a potential stagnation region near the source could be formed, as shown by Fig. 14a.

- To explain why FS-3 performs the best, we conducted three steady-state particle simulations for the three fan speeds. Fig. 15d compares the total particle counts of the fluid zone in the whole warehouse. It shows that FS-3 reaches steady-state around 200 mins, whereas the steady-state is not reached even at the end of the 8th hour for the two other cases, which again indicates a much slower mixing process in these two cases than FS-3.
- A shorter transient process is a result of a faster balance of particle generations and losses. The highest air velocity and the strongest dilution from FS-3 maximize the losses through both the doors and the surface deposition velocities and thus deposition rates. Therefore, FS-3 reaches the steady-state the fastest for the same particle generation rate with the lowest BZ concentration among all cases.
- Therefore, the BZ concentrations under various fan speeds are subject to the combined impacts of fan speeds, thermal buoyancy, and losses through surface depositions and doors. These combined impacts explain the higher concentration of FS-0.6 among all speeds.

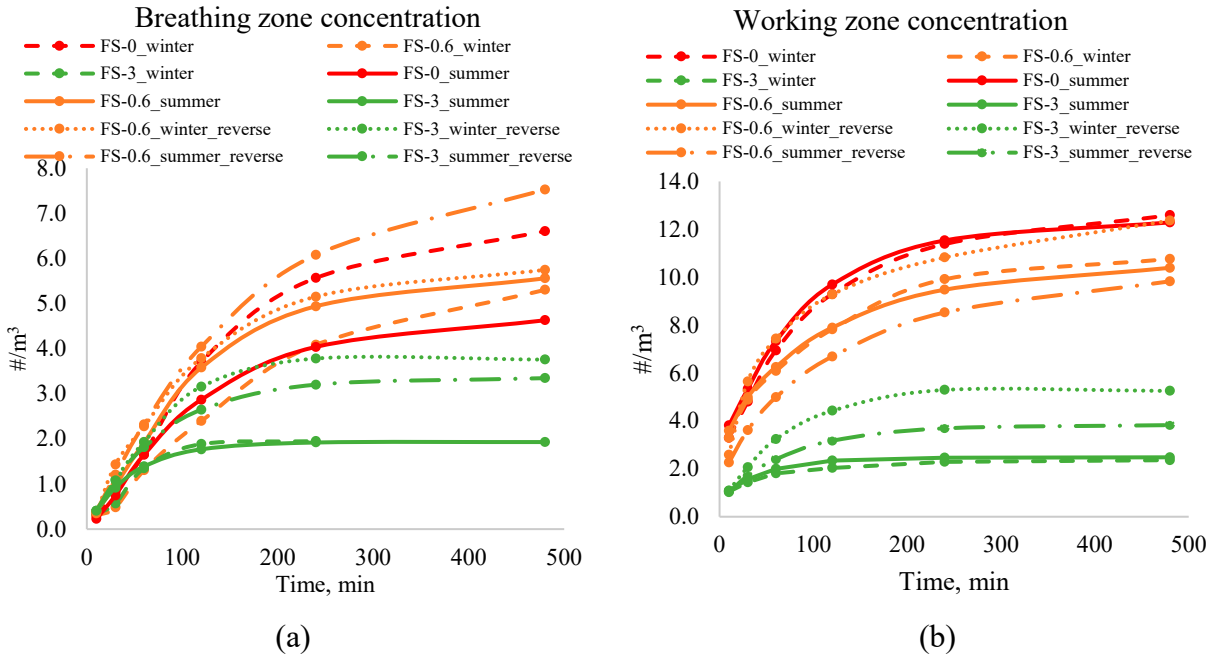

Figure 16. Comparison of concentration for the winter and summer conditions at the (a) Whole-warehouse Breathing Zone and (b) the Working Zone.

To investigate the impacts of different seasons, we conducted a series of simulations for the winter scenarios and compared the results to the summer cases in Fig. 16. There were no heating devices added to this case. The reason not to include heating devices is to avoid the local thermally-driven airflow patterns, which could be created from these heating devices so that the results may be case-dependent. The corresponding results without the heating devices are also associated with a stronger thermal buoyancy than with them. In other words, the impacts of the thermal buoyancy from workers could be overestimated in the current setup. Fig. 16 shows that FS-3 has a similar performance in both seasons, which is not surprising because of the dominating momentum-driven flows from the fan. The working zone concentrations for different fan speeds are not quite affected with the higher concentration in the summer than the winter for FS-0 and FS-3, whereas FS-0.6 has the lower concentration in the summer generally than in the winter. In the winter, all cases are with higher whole-warehouse breathing zone concentrations than in the summer except FS-0.6.

FS-0.6 (summer reverse) is with the highest level of breathing zone concentration among all scenarios. This indicates the importance of fan flows to create a certain level of "breeze". For FS-0.6, the whole-warehouse breathing zone concentration is lower in the winter case than the summer because of the stronger buoyancy-driven flows, as also previously shown in Figures 8 and 17. For FS-3, the whole warehouse is well mixed in both winter and summer cases, so the difference is minimal. Fig. 16 also shows that reversing the fan in the winter always causes higher concentrations in the breathing zone and working zone as a result of reduced airspeeds in the space and thus fewer particle losses. The Appendix compares the airflow and concentration distributions for both seasons after reversing the fan.

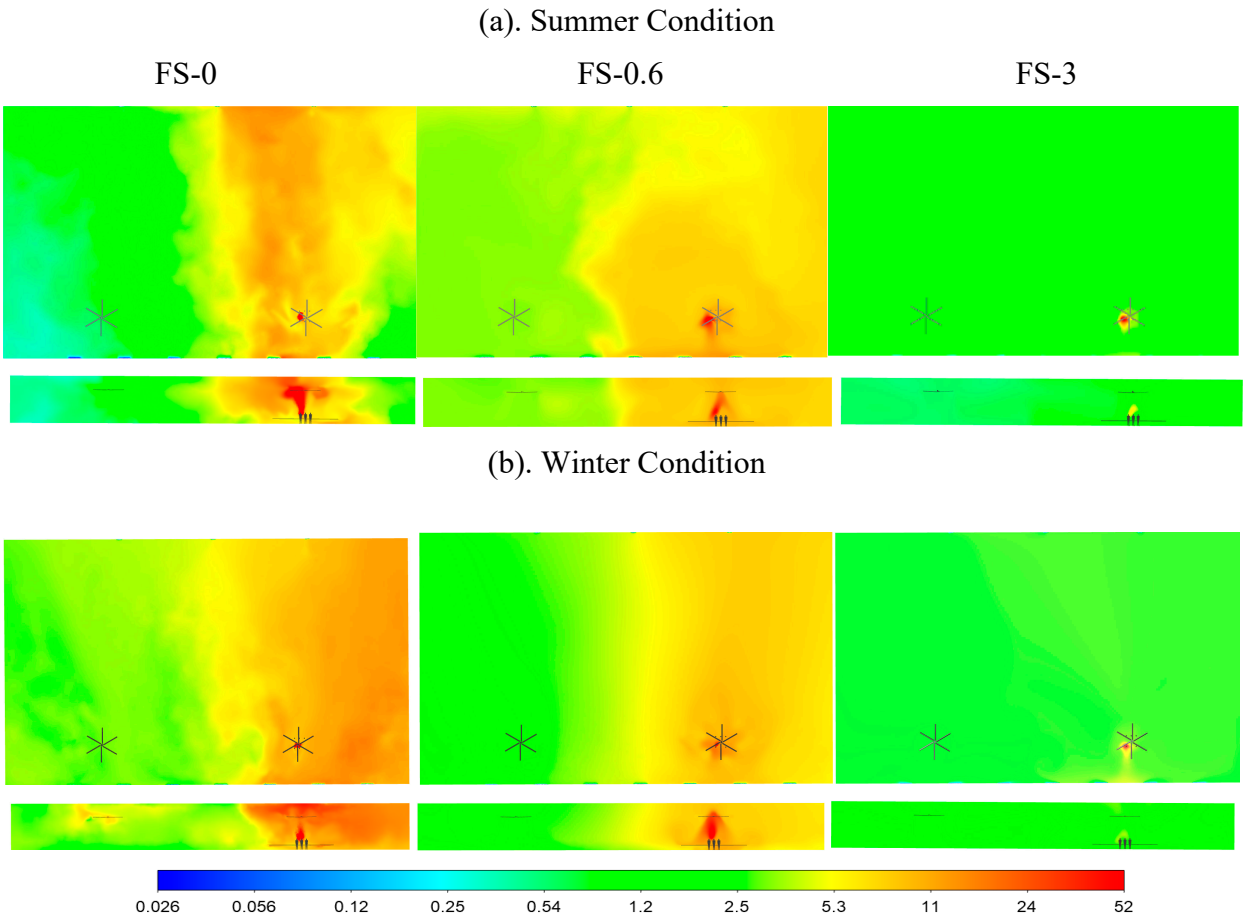

Figure 17. Comparison of the Whole-warehouse Breathing Zone concentrations (#/m^3) at the end of the 8th hour in the (a) Summer Condition and the (b) Winter Condition (U-H-D-3).

4.2 Impact of working area arrangement

- Whole Warehouse Breathing Zone Concentration

Figure 18 compares the impacts of the packing line and worker arrangements on the BZ concentrations. Each box chart column result shows the lowest, the highest, the average, the medium, the 25%, and 75% quantile concentrations among a total of eight cases. For example, the "bz_FS-0_V" is for the whole-warehouse breathing zone concentration of the eight FS-0 cases with the vertical packing line (see the 1st and 3rd rows in Fig. 10).

- The box charts show that FS-3 is always with the lowest BZ concentration regardless of the packing line direction and location or the worker locations;
- There is no noticeable difference for different packing line and worker arrangements for FS-0.6;
- For FS-0, the vertical packing line seems better than the horizontal, and placing the packing line in the middle of the two fans seems better than the other two placements; Single-row worker seems better than double row, and 6 ft distance is better than 3 ft, whereas the difference is not significant.

Impact of packing line location

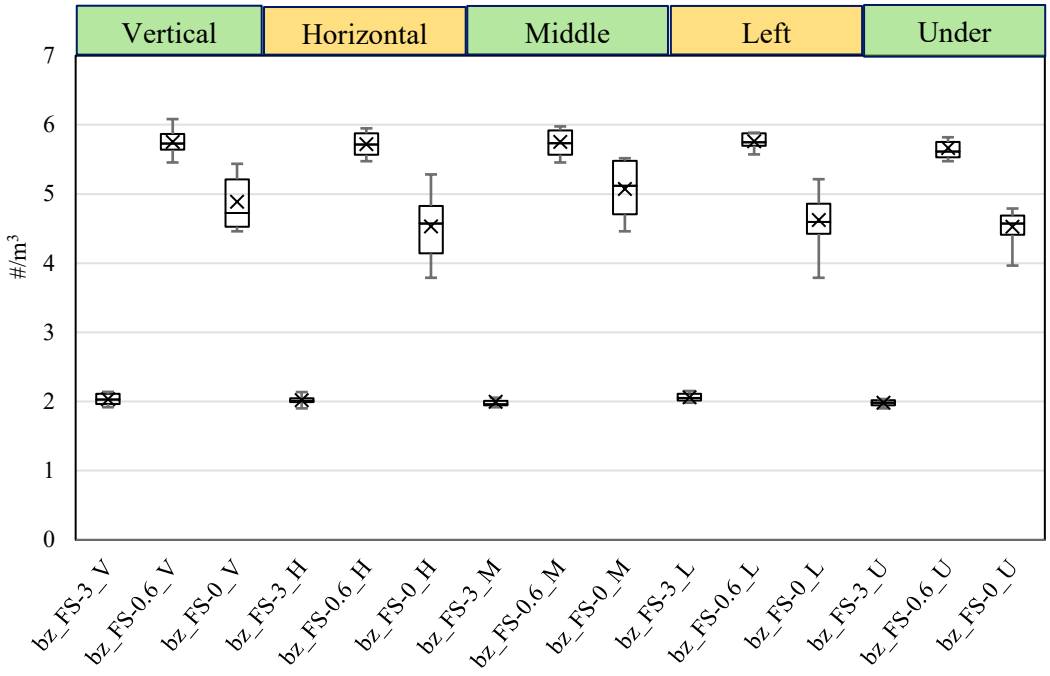

(a)

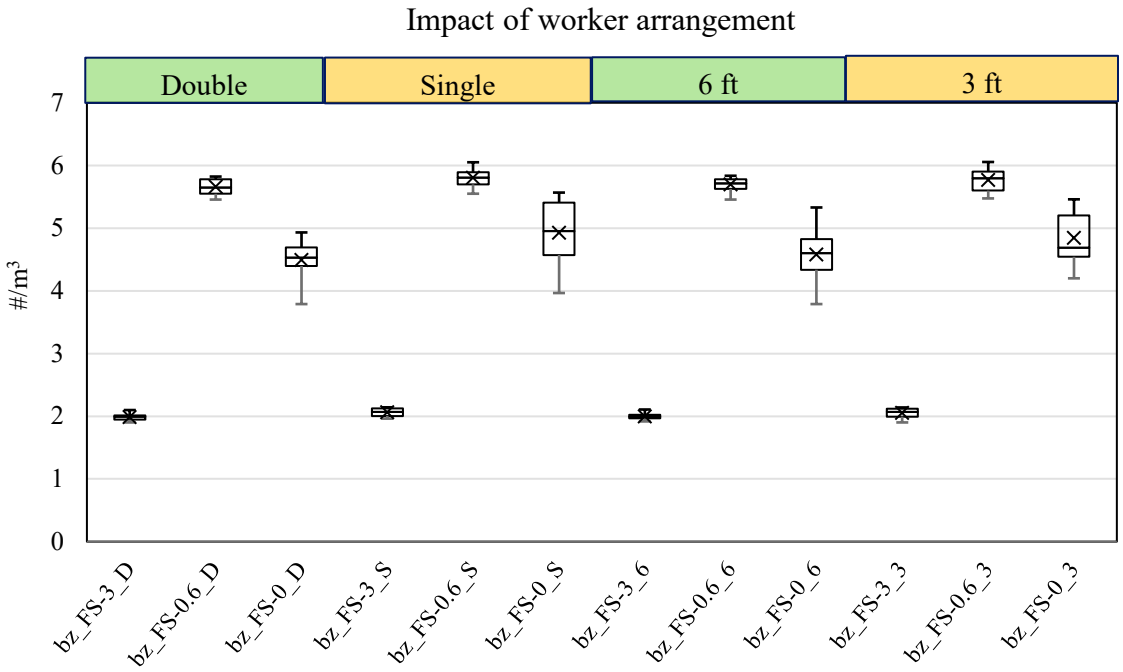

(b)

Figure 18. (a) Impact of packing line location and (b) impact of worker arrangement on the whole warehouse breathing zone concentrations for all cases (Summer).

- Working Zone Concentration

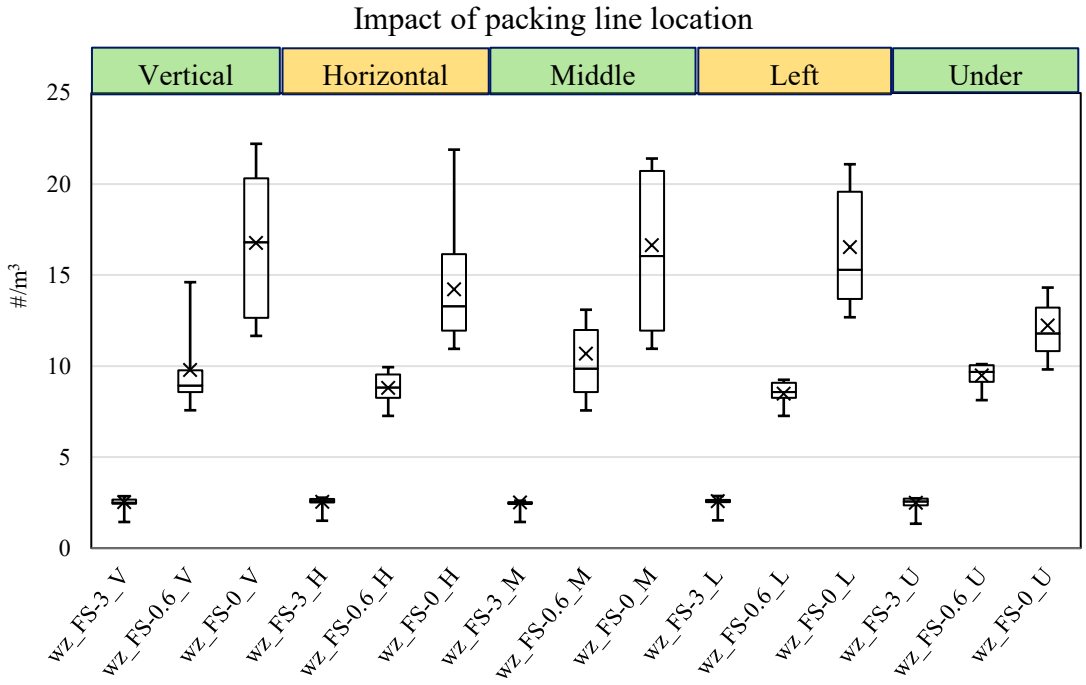

(a)

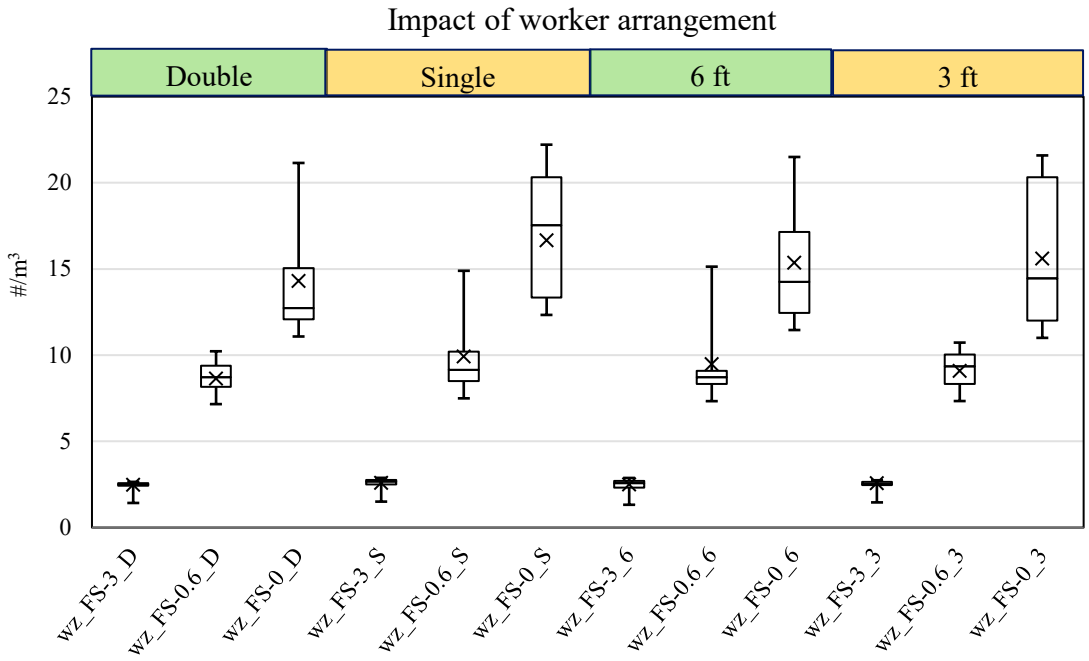

(b)

Figure 19. (a) Impact of packing line location and (b) impact of worker arrangement on the working zone concentrations for all cases (Summer).

For the working zone particle concentrations (Fig. 19),

- All FS-3 conditions have the minimum concentrations regardless of the packing line locations and work arrangements.
- For FS-0.6, the situation is complex, and no consistent conclusions can be drawn compared to the BZ cases: a wider band of variation is observed among different cases. However, all but one of the 16 scenarios show a reduction in concentration when comparing an FS-0.6 case to its otherwise identical FS-0 case. For FS-0, more variations are observed than FS-0.6 because the WZ concentrations could be subject to the combined impacts of multiple factors mentioned previously.

4.3 Impact of racks

Figure 20 compares the impact of racks for the BZ concentrations and the total fluid zone particle numbers for one selected case of L-V-D-6.

- For FS-3 and FS-0.6, the concentrations with the racks are close to those without them, while FS-0.6 has lower concentrations with the racks than without.
- For FS-0, the racks contribute to a lower concentration than the no-rack scenario, as both figures show. The racks seem to straighten the airflow in the E-W direction of the warehouse. The lower velocity inside the porous media region also slows down the spreading of particles in the warehouse resulting in a lower concentration in the whole warehouse. A visual comparison can be further examined for the results in the Appendix.

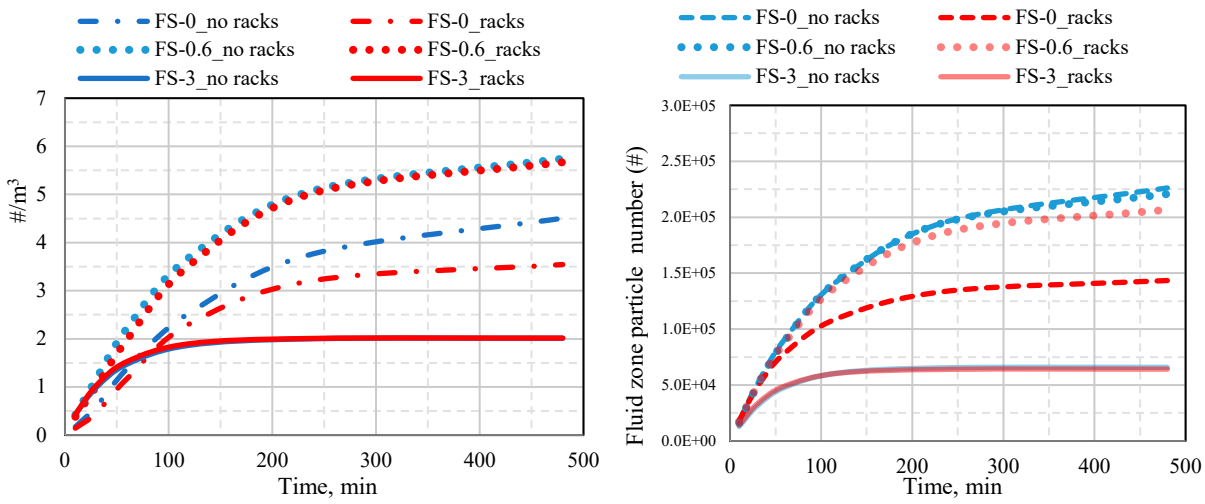

(a) (b)

Figure 20. Comparison of the transient (a) whole-warehouse breathing zone concentrations and (b) the fluid zone total particle counts with and without racks for L-V-D-6 (Summer).

5. CONCLUSIONS

This study investigated the transient particle dispersions in an industrial warehouse based on the US DOE warehouse reference building model when an infector releases particle source from loud speaking (shouting). 223 CFD simulations were conducted for different fan speed operations, working area and worker arrangements relative to the fans, and other simulations, including the impacts of thermal plumes, warehouse racks, and steady-state dispersions. The well-established Drift-flux model simulated particle dispersion and deposition. The fan rotation is modeled by the moving reference frame model. Both models were validated by the literature data.

Based on the parametric simulations, the following major conclusions are reached:

- Of the options for operating the fan (different speed or direction), operating the fans at the highest feasible speed consistently outperforms the other options.
- However, operating fans at the maximum speed generate high airspeeds in the occupied zone, which will not be practical in some conditions, for example, as it would cause thermal discomfort in cold indoor conditions. Where lower airspeeds are preferred: FS-3 reverse is a good option, although it is not as good as FS-3 with the downward flow.
- Reversing fans at higher fan speed (e.g., FS-3) reduces the performance compared to before reversing.
- Reversing fans at lower fan speed (e.g., FS-0.6) may reduce the whole warehouse airflow speed and thus lower diluting effect, so the whole warehouse concentration could become higher.
- The effects of thermal plumes from workers on the vertical particle spreading are significant, especially for still air cases; local air mixing and movement could help to dilute and reduce the chance of creating local hotspots

Based on the above conclusions, the following LDCF guideline is developed, which combines particle concentration considerations with thermal comfort constraints in practice. It is primarily intended for an audience of building operators or other individuals with control over the operation of fans in large spaces that are sparsely occupied.

Where are most occupants located?	Summer conditions	Winter conditions
Close to the fan(s)	Operate fans downwards, at high speed	Operate fans at the highest feasible speed that does not cause draft, in either forward or reverse, whichever approach was used pre-pandemic[1]
Far from the fan(s)[3]	Operate fans downwards, at high speed	Operate fans at the highest feasible speed, forward or reverse, whichever approach was used pre-pandemic[2]

Notes: Green/yellow/red color coding is an approximate indicator of how clear the effect was in the simulated scenarios.

1: Simulations show slightly lower concentrations for reverse vs. forward at the same low speed, but it is based on a much smaller number of simulated scenarios (2 vs. 16 for typical forward direction scenario) and is a small effect given simplifications and assumptions in the model, so we advise to retain the direction used pre-pandemic for simplicity. However, if reversing the fan allows for substantially higher fan speeds while avoiding draft at occupied level, then it is likely that this is the better option.

2: Simulations show a slight *increase* in average whole-warehouse breathing level concentration for fans at low-speed vs. off. However, the distribution is far more uniform across the entire warehouse (i.e., there are no "hot spots"). Based on feedback from the science team, overall, this homogeneity is still likely a net advantage. Because although people may be far apart a lot of the time, they will still meet and interact more closely during the workday, and here more mixing (i.e., dilution) is beneficial. Lastly, the still air results depend highly on model assumptions and simplifications (e.g., the effectiveness of plume, lack of local mixing, racks present vs. not, etc.), and this small difference could be an artifact of those.

3: For context, "far from the fans" could be defined as when most occupants spend the majority of the day at locations more than three fan diameters from the center of a fan.

A simplified version of the guideline is also included:

- Primary target audience: building operator in a facility with existing fans, or (secondary) a designer
- Where feasible, open doors or windows and operate fans as they will increase ventilation airflow through these openings.
- Avoid locating occupants immediately downstream of each other for extended time periods.
- Operate fans at the highest feasible speed while maintaining occupant comfort in the space.
- At high fan speeds (e.g., summer conditions), the simulations show a notable reduction in concentration
- At low fan speed, the simulations show a slight reduction in concentration in the region close to the fan (e.g., within two fan diameters) and no practical difference outside that region.

6. LIMITATIONS

The data, results, conclusions, and guidelines in this report were obtained based on the numerical simulations, subject to underlying assumptions as presented in Section 2.5 of this report, so a few limitations are summarized:

- The proposed LDCF guidelines are based on the relative reduction of the BZ and WZ particle concentration levels. Therefore, they do not imply any safe/unsafe conditions but suggest the fan operation strategy for a relatively lower particle concentration in the space.
- The results for the still air (FS-0) cases are more dependent on the assumptions than the FS > 0 cases, as the fan momentum-driven airflows tend to dominate the air distribution in the space when the fan operates. Therefore, a slight change to these assumptions (less effective thermal plume, more mixing effects from people/vehicles movements, different or unsteady ventilation flows through windows and doors) could have a relatively large impact on these FS-0 cases' results which would affect the overall conclusions.
- As we have modeled, the significant reduction in concentrations for the FS-3 scenarios is primarily due to dilution and losses through depositions. So, the results depend on the accuracy of the deposition model, without which the predicted concentrations would be higher, and the conclusions could be different.
- The warehouse of interest has a large volume space and is sparsely occupied, so the conclusions may not apply to other cases otherwise, such as a space with a small volume and/or densely occupied.

7. ACKNOWLEDGMENTS

Science Team for AMCA LDCF COVID Guidance Research			
Liangzhu (Leon) Wang, PhD	Associate Professor, Building, Civil, and Environmental Engineering	Concordia University, Montreal	Principal Investigator
William P. Bahnfleth, PhD, PE, FASHRAE	Professor of Architectural Engineering	The Pennsylvania State University	Chair of ASHRAE Epidemic Task Force and research guidance
Edward. Nardell, PhD	Professor in the Departments of Environmental Health and Immunology and Infectious Diseases, Harvard University	Harvard T. H. Chan School of Public Health	Infectious diseases and study of ceiling fans for control of infectious diseases
Jovan Pantelic, PhD	Research Scientist, Building Science	Well Living Lab	Infectious diseases
Paul Raftery, PhD	Professional Researcher	University of California Berkeley Center for the Built Environment	Ceiling fan modeling
Geoffrey Sheard, PhD	President	AGS Consulting	Computational fluid dynamics modeling and fan engineering
Pawel Wargocki, PhD	Associate Professor	Technical University of Denmark	Chair of ASHRAE ETF Science Applications

			Committee. Indoor air quality expertise
Industry Team for AMCA LDCF COVID Guidance Research			
Michael Ivanovich	Senior Director, Global Relations	AMCA International	Project Manager
Eddie Boyd	President and CEO	Macroair	LDCF performance
Marc Brandt	Director, Domestic Industrial Business	Hunter Industrial	LDCF Performance
Thomas Catania, Esq.	Board Member	Institute for Energy Innovation	Regulatory communications
Mark Stevens	Executive Director	AMCA International	Member relations
Christian Taber	Principal Engineer	Big Ass Fans	Warehouse model, LDCF modeling
Mike Wolf	Director, Regulatory Business Development	Greenheck Fan	Regulatory communications

The project is funded by Air Movement and Control Association (AMCA). We acknowledge the valuable inputs from Dr. Paul Raftery, Michael Ivanovich, Christian Taber, and many others from AMCA. Dr. Raftery and Dr. Wang drafted the AMCA LDCF guidelines with many inputs from Mr. Taber and Dr. Edward Nardell from the Harvard T.H. Chan School of Public Health. Thanks to the science team, including Dr. William Bahnfleth from Pennsylvania State University, Dr. Pawel Wargocki at the Technical University of Denmark, and Dr. Jovan Pantelic from Well Living Lab. We also acknowledge the support from Dr. Naiping Gao from Tongji University, China, for sharing his team's work on the ANSYS FLUENT UDFs. The project is made possible by the Concordia University High-Performance Computing cluster SPEED. All the contributors with the roles and expertise are included in the above table.

8. DISCLAIMER

Users are advised to interpret, use, and apply the results, conclusions, and guidelines with caution. The authors are not responsible for any adverse outcomes because of users' interpretation and applications of the information provided in this report.

9. REFERENCES

[1] WHO, WHO Coronavirus (COVID-19) Dashboard | WHO Coronavirus (COVID-19) Dashboard With Vaccination Data, (2021). https://covid19.who.int/ (accessed August 9, 2021).

[2] L. Morawska, J. Cao, Airborne transmission of SARS-CoV-2: The world should face the reality, Environ. Int. (2020). https://doi.org/10.1016/j.envint.2020.105730.

[3] S. Asadi, N. Bouvier, A.S. Wexler, W.D. Ristenpart, The coronavirus pandemic and aerosols: Does COVID-19 transmit via expiratory particles?, Aerosol Sci. Technol. (2020). https://doi.org/10.1080/02786826.2020.1749229.

[4] S. Tang, Y. Mao, R.M. Jones, Q. Tan, J.S. Ji, N. Li, J. Shen, Y. Lv, L. Pan, P. Ding, X.

Wang, Y. Wang, C.R. MacIntyre, X. Shi, Aerosol transmission of SARS-CoV-2? Evidence, prevention and control, Environ. Int. (2020). https://doi.org/10.1016/j.envint.2020.106039.

[5] S.L. Miller, W.W. Nazaroff, J.L. Jimenez, A. Boerstra, G. Buonanno, S.J. Dancer, J. Kurnitski, L.C. Marr, L. Morawska, C. Noakes, Transmission of SARS-CoV-2 by inhalation of respiratory aerosol in the Skagit Valley Chorale superspreading event, MedRxiv. (2020). https://doi.org/10.1101/2020.06.15.20132027.

[6] E.L. Anderson, P. Turnham, J.R. Griffin, C.C. Clarke, Consideration of the Aerosol Transmission for COVID-19 and Public Health, Risk Anal. (2020). https://doi.org/10.1111/risa.13500.

[7] R. Zhang, Y. Li, A.L. Zhang, Y. Wang, M.J. Molina, Identifying airborne transmission as the dominant route for the spread of COVID-19, Proc. Natl. Acad. Sci. U. S. A. (2020). https://doi.org/10.1073/pnas.2009637117.

[8] L. Morawska, J.W. Tang, W. Bahnfleth, P.M. Bluyssen, A. Boerstra, G. Buonanno, J. Cao, S. Dancer, A. Floto, F. Franchimon, C. Haworth, J. Hogeling, C. Isaxon, J.L. Jimenez, J. Kurnitski, Y. Li, M. Loomans, G. Marks, L.C. Marr, L. Mazzarella, A.K. Melikov, S. Miller, D.K. Milton, W. Nazaroff, P. V Nielsen, C. Noakes, J. Peccia, X. Querol, C. Sekhar, O. Seppänen, S. ichi Tanabe, R. Tellier, K.W. Tham, P. Wargocki, A. Wierzbicka, M. Yao, How can airborne transmission of COVID-19 indoors be minimised?, Environ. Int. (2020). https://doi.org/10.1016/j.envint.2020.105832.

[9] M.A. Kohanski, L.J. Lo, M.S. Waring, Review of indoor aerosol generation, transport, and control in the context of COVID-19, Int. Forum Allergy Rhinol. (2020). https://doi.org/10.1002/alr.22661.

[10] P. Raftery, J. Fizer, W. Chen, Y. He, H. Zhang, E. Arens, S. Schiavon, G. Paliaga, Ceiling fans: Predicting indoor air speeds based on full scale laboratory measurements, Build. Environ. 155 (2019) 210–223.

[11] W. Chen, H. Zhang, E. Arens, M. Luo, Z. Wang, L. Jin, J. Liu, F.S. Bauman, P. Raftery, Ceiling-fan-integrated air conditioning: Airflow and temperature characteristics of a sidewall-supply jet interacting with a ceiling fan, Build. Environ. (2020). https://doi.org/10.1016/j.buildenv.2020.106660.

[12] Y. Gao, H. Zhang, E. Arens, E. Present, B. Ning, Y. Zhai, J. Pantelic, M. Luo, L. Zhao, P. Raftery, S. Liu, Ceiling fan air speeds around desks and office partitions, Build. Environ. (2017). https://doi.org/10.1016/j.buildenv.2017.08.029.

[13] H. Wang, M. Luo, G. Wang, X. Li, Airflow pattern induced by ceiling fan under different rotation speeds and blowing directions, Indoor Built Environ. (2020). https://doi.org/10.1177/1420326X19890054.

[14] E. Present, P. Raftery, G. Brager, L.T. Graham, Ceiling fans in commercial buildings: In situ airspeeds & practitioner experience, Build. Environ. (2019). https://doi.org/10.1016/j.buildenv.2018.10.012.

[15] R. Bassiouny, N.S. Korah, Studying the features of air flow induced by a room ceiling-fan, Energy Build. (2011). https://doi.org/10.1016/j.enbuild.2011.03.034.

[16] S. Zhu, J. Srebric, S.N. Rudnick, R.L. Vincent, E.A. Nardell, Numerical modeling of indoor environment with a ceiling fan and an upper-room ultraviolet germicidal irradiation system, Build. Environ. 72 (2014) 116–124. https://doi.org/10.1016/j.buildenv.2013.10.019.

[17] W. Li, A. Chong, T. Hasama, L. Xu, B. Lasternas, K.W. Tham, K.P. Lam, Effects of ceiling fans on airborne transmission in an air-conditioned space, Build. Environ. (2021). https://doi.org/10.1016/j.buildenv.2021.107887.

[18] B.A. Craven, G.S. Settles, A Computational and Experimental Investigation of the Human Thermal Plume, J. Fluids Eng. (2006). https://doi.org/10.1115/1.2353274.

[19] S. Asadi, A.S. Wexler, C.D. Cappa, S. Barreda, N.M. Bouvier, W.D. Ristenpart, Aerosol emission and superemission during human speech increase with voice loudness, Sci. Rep. 9 (2019) 1–10. https://doi.org/10.1038/s41598-019-38808-z.

[20] H. Dai, B. Zhao, Association of infected probability of COVID-19 with ventilation rates in confined spaces: A Wells-Riley equation based investigation, MedRxiv. (2020) 1321–1327. https://doi.org/10.1101/2020.04.21.20072397.

[21] Z.T. Ai, A.K. Melikov, Airborne spread of expiratory droplet nuclei between the occupants of indoor environments: A review, Indoor Air. 28 (2018) 500–524. https://doi.org/10.1111/ina.12465.

[22] S. Shao, D. Zhou, R. He, J. Li, S. Zou, K. Mallery, S. Kumar, S. Yang, J. Hong, Risk assessment of airborne transmission of COVID-19 by asymptomatic individuals under different practical settings, ArXiv. 19 (2020) 1–29.

[23] N.P. Gao, J.L. Niu, Modeling particle dispersion and deposition in indoor environments, Atmos. Environ. 41 (2007) 3862–3876. https://doi.org/10.1016/j.atmosenv.2007.01.016.

[24] J.A. Adeniran, I.A. Mohammed, O.I. Muniru, T. Oloyede, O.O. Sonibare, M.N.O. Yusuf, K.A. Abdulraheem, E.T. Odediran, R.O. Yusuf, J.A. Sonibare, Indoor transmission dynamics of expired SARS-CoV-2 virus in a model African hospital ward, J. Environ. Heal. Sci. Eng. (2021). https://doi.org/10.1007/s40201-020-00606-5.

[25] J. FAN, L.U. TIAN, X. JIA, THE NUMERICAL STUDY WITH DYNAMIC MESH ON THE POLLUTION CONTROL EFFECT OF OPERATING TABLE PROTECTED BY LAMINAR FLOW SCREEN, Int. J. Mod. Phys. Conf. Ser. (2016). https://doi.org/10.1142/s2010194516601563.

[26] J. Fan, X. Yang, S. Wang, X. Zheng, Numerical study on effect of operating table protected by horizontal laminar flow screen, Trans. Nanjing Univ. Aeronaut. Astronaut. (2013).

[27] J. Hang, Y. Li, R. Jin, The influence of human walking on the flow and airborne transmission in a six-bed isolation room: Tracer gas simulation, Build. Environ. (2014). https://doi.org/10.1016/j.buildenv.2014.03.029.

[28] Z. Li, H. Wang, W. Zheng, B. Li, Y. Wei, J. Zeng, C. Lei, A tracing method of airborne bacteria transmission across built environments, Build. Environ. (2019). https://doi.org/10.1016/j.buildenv.2019.106335.

[29] Y. Li, H. Qian, J. Hang, X. Chen, P. Cheng, H. Ling, S. Wang, P. Liang, J. Li, S. Xiao, J.

Wei, L. Liu, B.J. Cowling, M. Kang, Probable airborne transmission of SARS-CoV-2 in a poorly ventilated restaurant, Build. Environ. (2021). https://doi.org/10.1016/j.buildenv.2021.107788.

[30] J.R. Andrews, C. Morrow, R. Wood, Modeling the role of public transportation in sustaining tuberculosis transmission in South Africa, Am. J. Epidemiol. (2013). https://doi.org/10.1093/aje/kws331.

[31] Z. Ai, C.M. Mak, N. Gao, J. Niu, Tracer gas is a suitable surrogate of exhaled droplet nuclei for studying airborne transmission in the built environment, Build. Simul. (2020). https://doi.org/10.1007/s12273-020-0614-5.

[32] H. Jin, Y. Chen, Q. Li, J. Fan, K. Luo, Numerical prediction of indoor airborne particle concentration in a test chamber with drift-flux model, J. Therm. Sci. (2011). https://doi.org/10.1007/s11630-011-0452-y.

[33] H. Jin, C. He, L. Lu, J. Fan, Numerical investigation of the wall effect on airborne particle dispersion in a test chamber, Aerosol Air Qual. Res. (2013). https://doi.org/10.4209/aaqr.2012.04.0106.

[34] A.C.K. Lai, W.W. Nazaroff, Modeling indoor particle deposition from turbulent flow onto smooth surfaces, J. Aerosol Sci. (2000). https://doi.org/10.1016/S0021-8502(99)00536-4.

[35] ANSYS Inc., ANSYS Fluent 2020R2 User's Guide, 2020.

[36] Z. Zhang, Q. Chen, Experimental measurements and numerical simulations of particle transport and distribution in ventilated rooms, Atmos. Environ. (2006). https://doi.org/10.1016/j.atmosenv.2006.01.014.

[37] C. Paper, S. Catarina, CFD Applied to the Investigation of Flow Resistances in Porous Media CFD Applied to the Investigation of Flow Resistances in, (2015).

[38] Y. Umeda, F. Ishida, M. Tsuji, K. Furukawa, M. Shiba, R. Yasuda, N. Toma, H. Sakaida, H. Suzuki, Computational fluid dynamics (CFD) using porous media modeling predicts recurrence after coiling of cerebral aneurysms, PLoS One. 12 (2017). https://doi.org/10.1371/journal.pone.0190222.

[39] A.O. Mahgoub, S. Ghani, Numerical and experimental investigation of utilizing the porous media model for windbreaks CFD simulation, Sustain. Cities Soc. (2021). https://doi.org/10.1016/j.scs.2020.102648.

[40] G. Nelson, Development of an experimentally-validated compact model of a server rack: Master Thesis, (2007) 150.

[41] A. Ambaw, P. Verboven, T. Defraeye, E. Tijskens, A. Schenk, U.L. Opara, B.M. Nicolai, Porous medium modeling and parameter sensitivity analysis of 1-MCP distribution in boxes with apple fruit, J. Food Eng. (2013). https://doi.org/10.1016/j.jfoodeng.2013.05.007.

[42] E. Bjørn, P. V Nielsen, Dispersal of exhaled air and personal exposure in displacement ventilated rooms, Indoor Air. (2002). https://doi.org/10.1034/j.1600-0668.2002.08126.x.

[43] H. Brohus, Personal exposure in displacement ventilated rooms, Indoor Air. (1996). https://doi.org/10.1111/j.1600-0668.1996.t01-1-00003.x.

[44] C.Y.H. Chao, M.P. Wan, L. Morawska, G.R. Johnson, Z.D. Ristovski, M. Hargreaves, K. Mengersen, S. Corbett, Y. Li, X. Xie, D. Katoshevski, Characterization of expiration air jets and droplet size distributions immediately at the mouth opening, J. Aerosol Sci. (2009). https://doi.org/10.1016/j.jaerosci.2008.10.003.

[45] Z.T. Ai, T. Huang, A.K. Melikov, Airborne transmission of exhaled droplet nuclei between occupants in a room with horizontal air distribution, Build. Environ. (2019). https://doi.org/10.1016/j.buildenv.2019.106328.

[46] A.C. Fears, R.F. Garry, C.J. Roy, D.S. Reed, W.B. Klimstra, P. Duprex, A. Hartman, S.C. Weaver, K.C. Plante, D. Mirchandani, J.A. Plante, P. V Aguilar, D. Fernández, A. Nalca, A. Totura, D. Dyer, B. Kearney, M. Lackemeyer, J.K. Bohannon, R. Johnson, Comparative dynamic aerosol efficiencies of three emergent coronaviruses and the unusual persistence of SARS-CoV-2 in aerosol suspensions, MedRxiv Prepr. Serv. Heal. Sci. (2020). https://doi.org/10.1101/2020.04.13.20063784.

[47] Ashrae Standard, ASHRAE Handbook Fundamentals 2017, Ashrae. (2017).

[48] J. Liu, S. Zhu, M.K. Kim, J. Srebric, A review of CFD analysis methods for personalized ventilation (PV) in indoor built environments, Sustain. (2019). https://doi.org/10.3390/su11154166.

10.Appendix

- Impact of particle diameters (U-H-D-3, FS-3)

The particle concentration for different particle diameters in the Whole-warehouse Breathing Zone and the Working Zone (U-H-D-3, FS-3) (Summer).

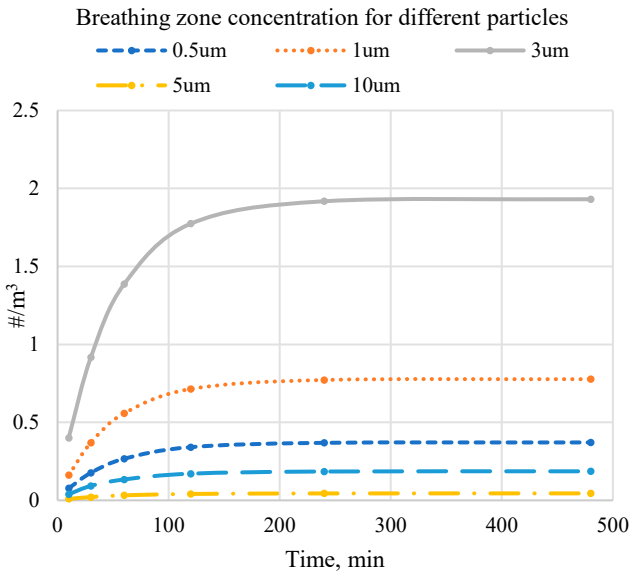

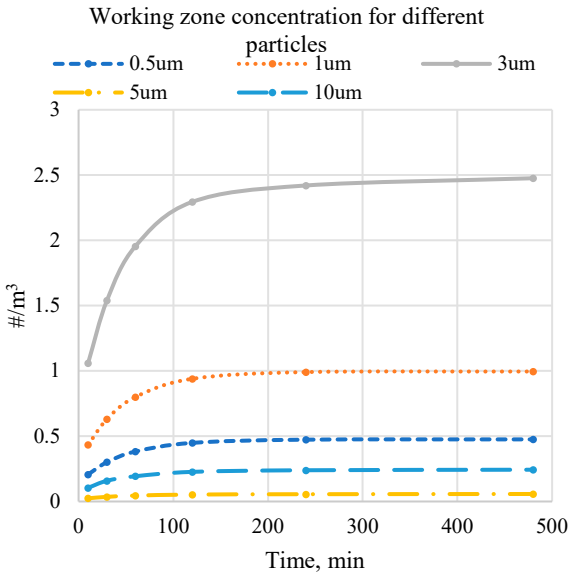

- Steady-state airflow distributions at the whole-warehouse breathing zones for all cases

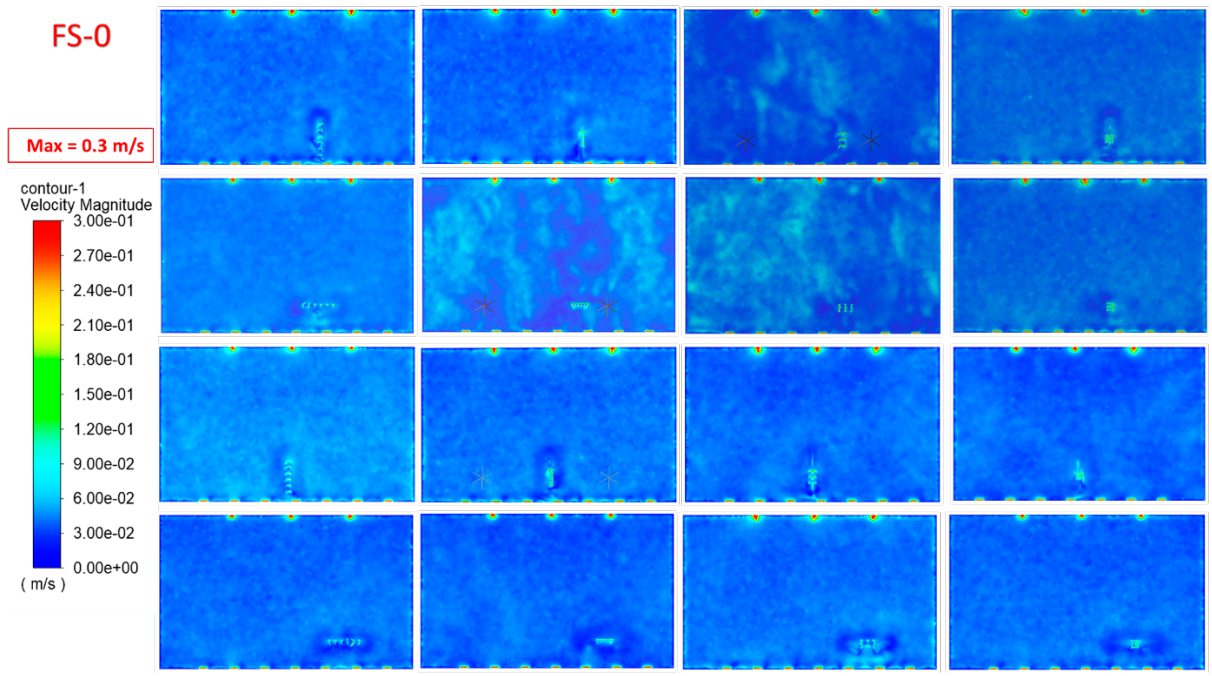

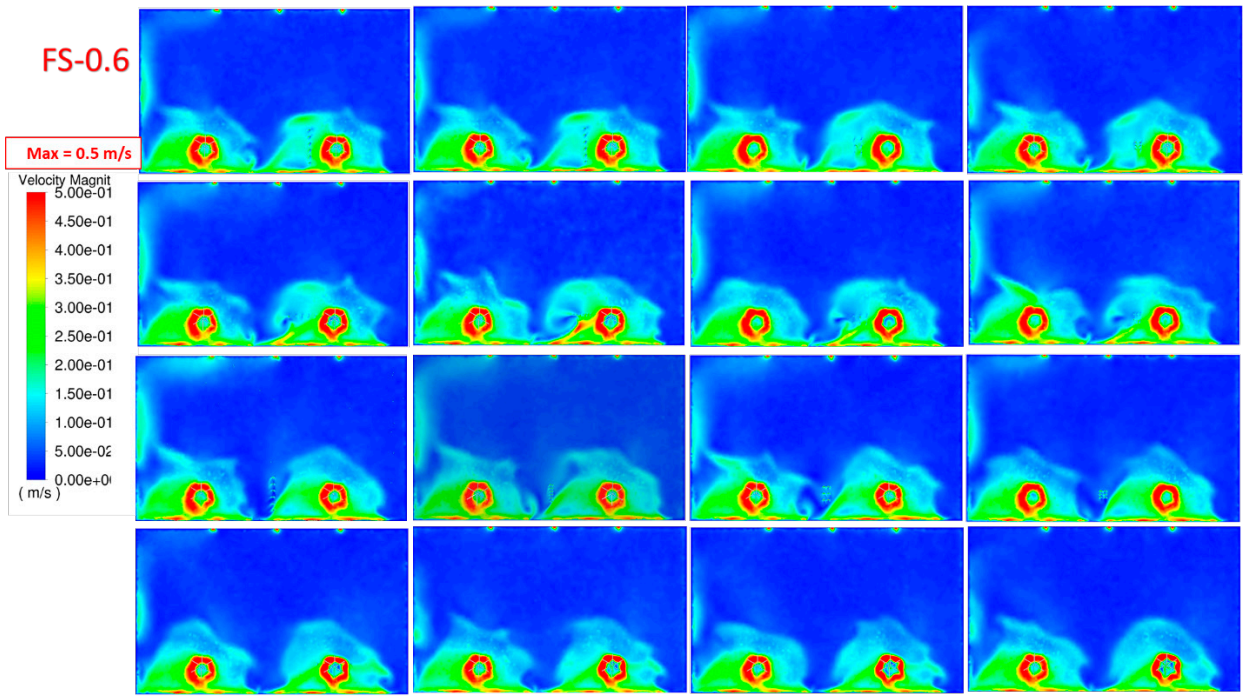
FS-0.6
Max = 0.5 m/s
Velocity Magnit
5.00e-01
4.50e-01
4.00e-01
3.50e-01
3.00e-01
2.50e-01
2.00e-01
1.50e-01
1.00e-01
5.00e-02
0.00e+00
(m/s)

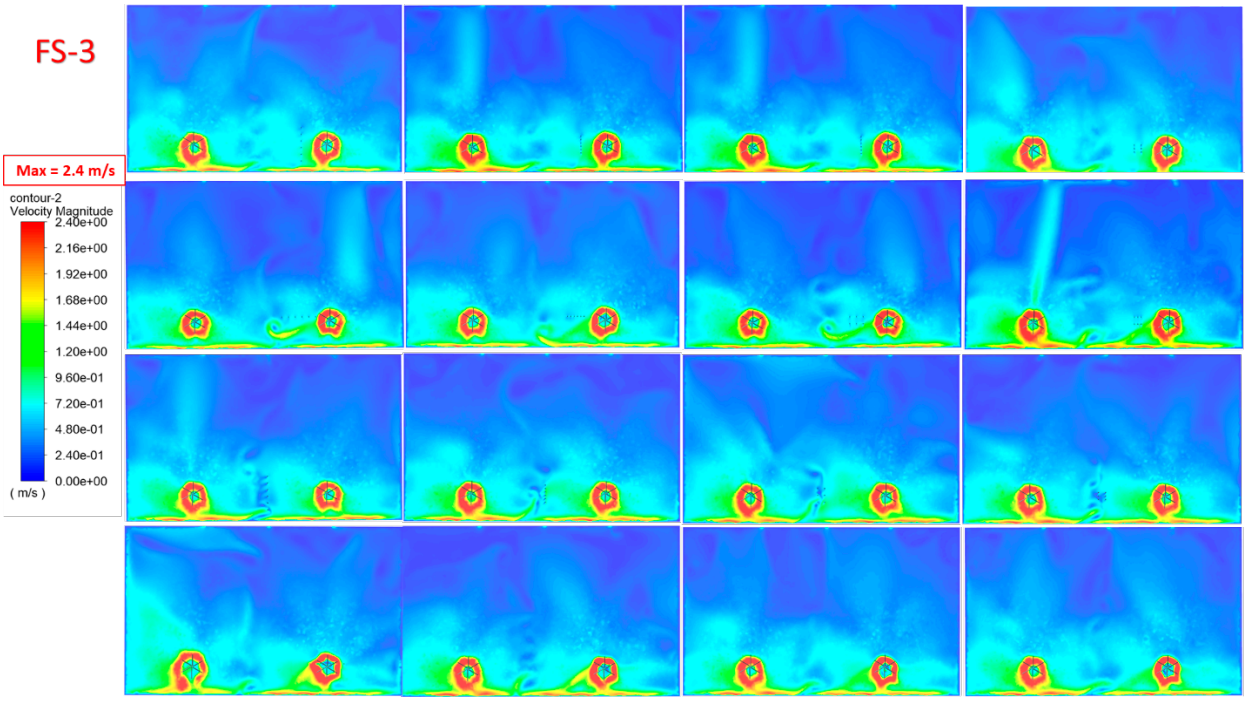
FS-3
Max = 2.4 m/s
contour-2
Velocity Magnitude
2.40e+00
2.16e+00
1.92e+00
1.68e+00
1.44e+00
1.20e+00
9.60e-01
7.20e-01
4.80e-01
2.40e-01
0.00e+00
(m/s)

- Impact of racks (L-V-D-6)

Whole warehouse breathing zone particle concentration at the end of the 8th hour

- Full fan speed – FS-3

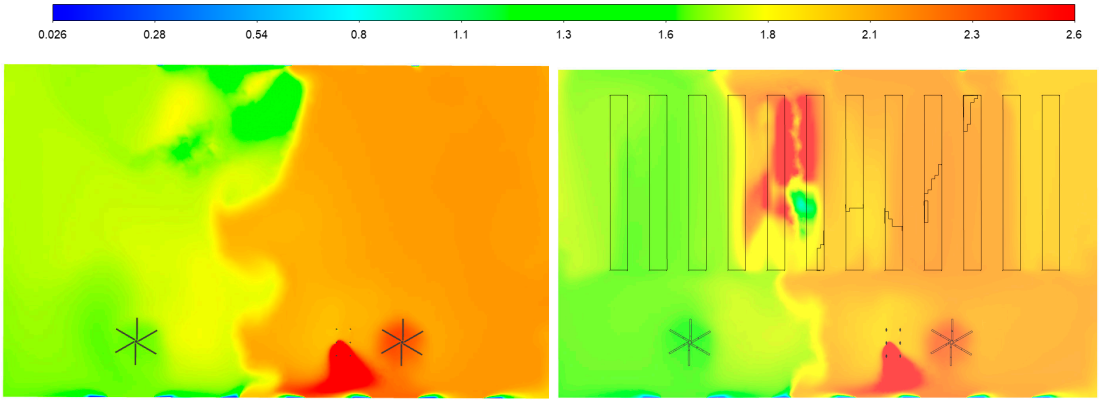

- 20% fan speed – FS-0.6

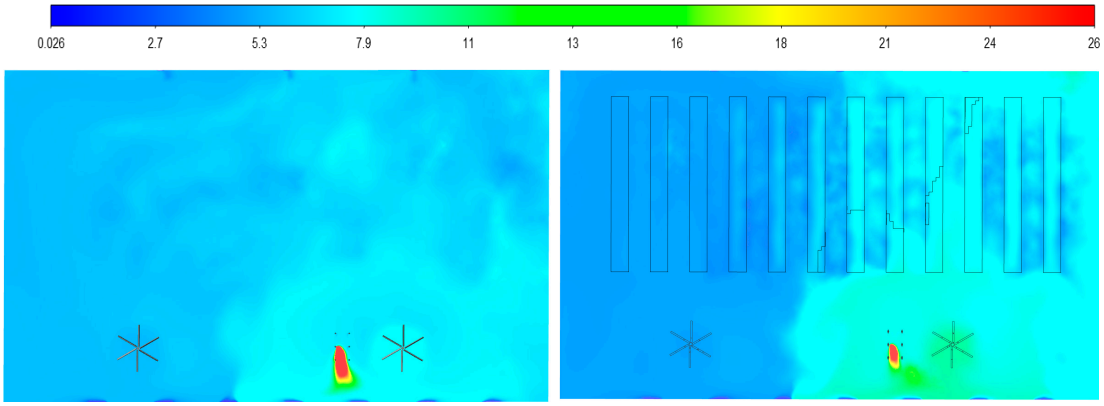

- Fan off – FS-0

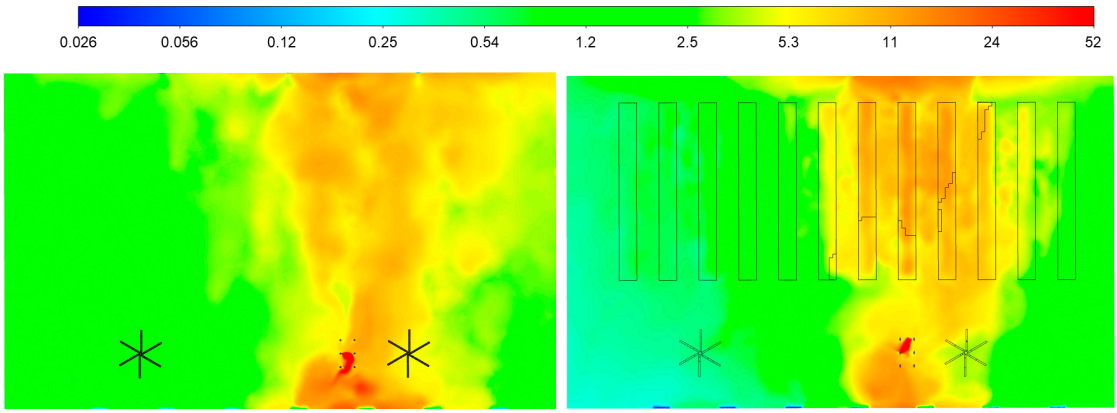

- Impact of wall temperatures in the winter

  - Airflow patterns for different winter surface temperature settings (U-H-D-3, FS-3)

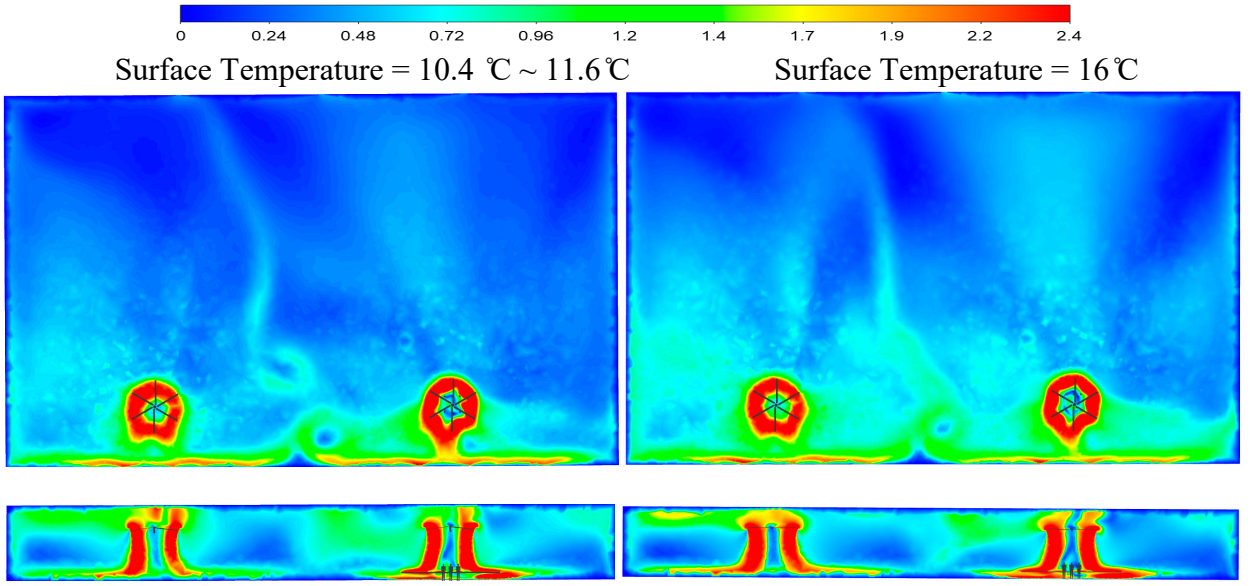

  - Concentration distributions for different winter surface temperatures (U-H-D-3, FS-3)

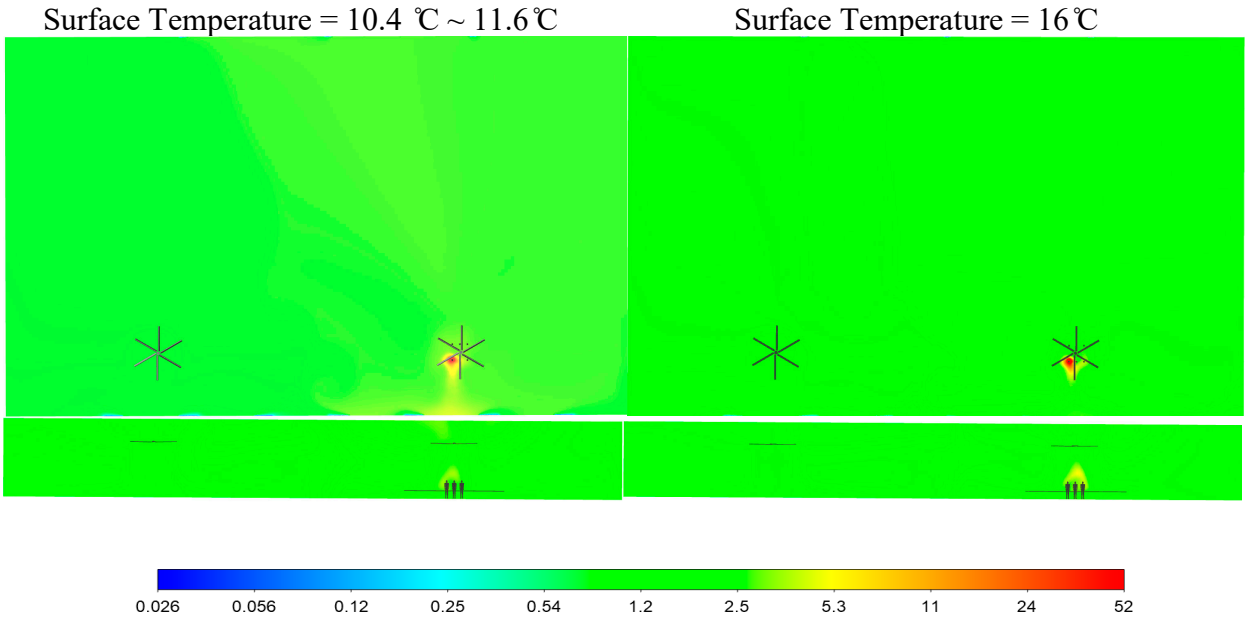

- Impact of fan reversing
  - Airflow patterns for reversing fan in the summer (U-H-D-3)

FS-0.6_reverse FS-3_reverse

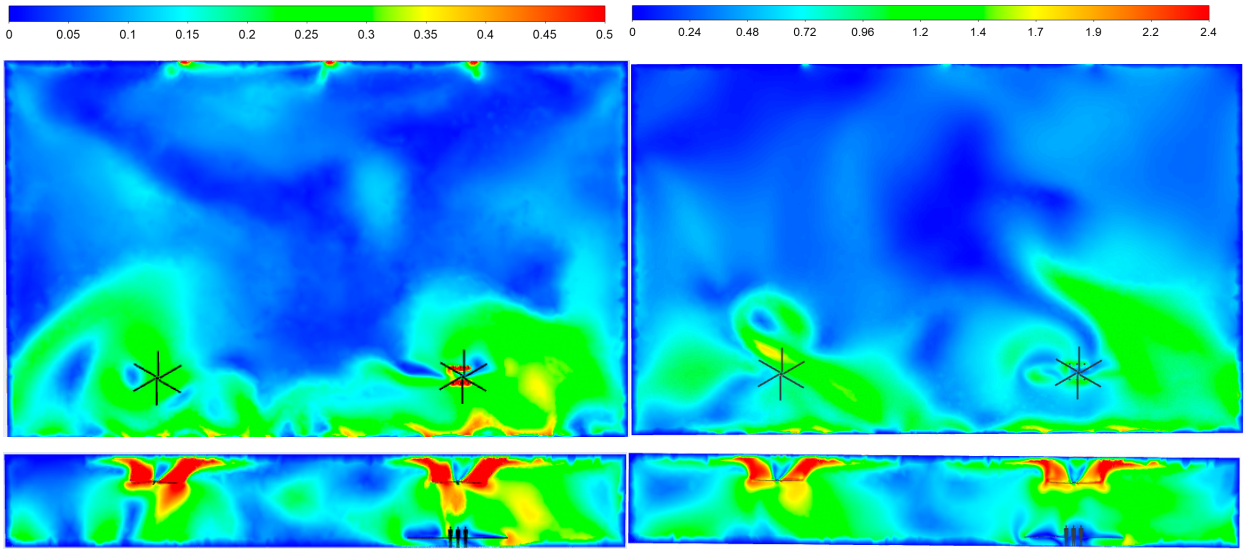

  - Airflow patterns for reversing fan in the winter (U-H-D-3)

FS-0.6_reverse FS-3_reverse

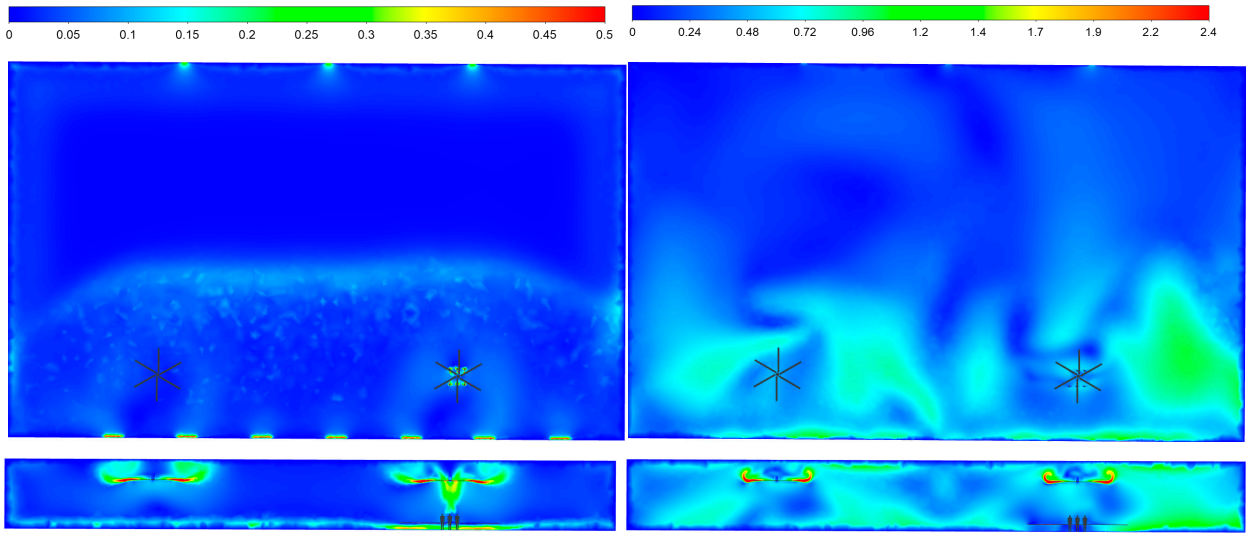

○ Concentration distributions when reversing fans in the summer (U-H-D-3)

FS-0.6_reverse FS-3_reverse

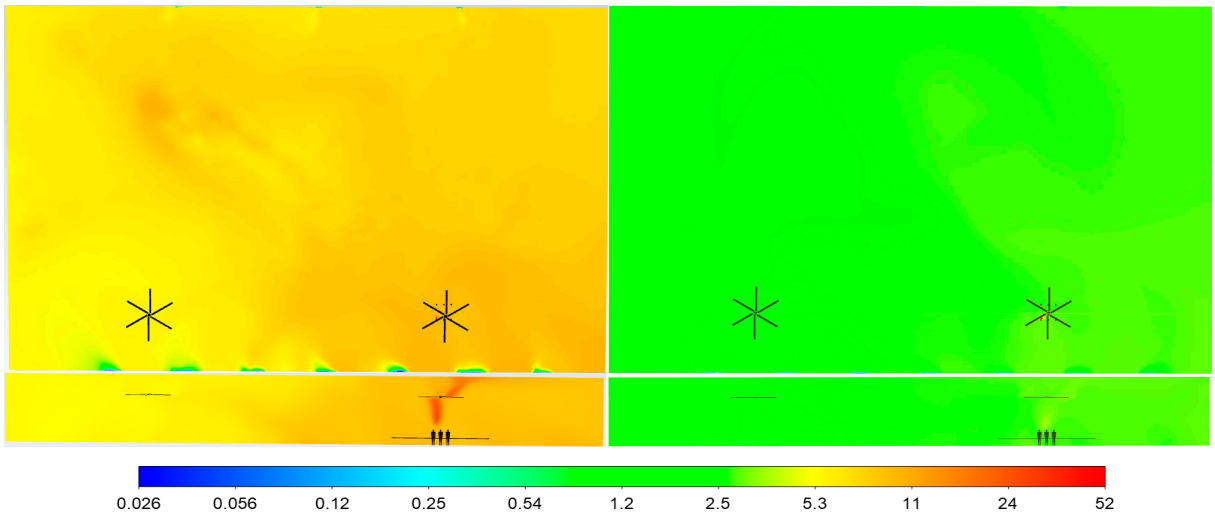

○ Concentration distributions when reversing fans in the summer (U-H-D-3)

FS-0.6_reverse FS-3_reverse